

1 **Evaluation of Anthropogenic Emissions and Ozone Pollution in the North China Plain:**  
2 **Insights from the Air Chemistry Research in Asia (ARIAs) Campaign**

3  
4 Hao He<sup>1</sup>, Xinrong Ren<sup>1,2,3</sup>, Sarah E. Benish<sup>1</sup>, Zhanqing Li<sup>1,4,5</sup>, Fei Wang<sup>5,6</sup>, Yuying Wang<sup>5</sup>,  
5 Timothy P. Canty<sup>1</sup>, Xiaobo Dong<sup>7</sup>, Feng Lv<sup>7</sup>, Yongtao Hu<sup>8</sup>, Tong Zhu<sup>9</sup>, and Russell R.  
6 Dickerson,<sup>1,4</sup>

7  
8 <sup>1</sup>Department of Atmospheric and Oceanic Science, University of Maryland, College Park, MD  
9 20742, USA

10 <sup>2</sup>Air Resources Laboratory, National Oceanic and Atmospheric Administration, College Park,  
11 MD 20742, USA

12 <sup>3</sup>Cooperative Institute for Climate and Satellites, University of Maryland, College Park,  
13 Maryland, USA

14 <sup>4</sup>Earth System Science Interdisciplinary Center, University of Maryland, College Park, MD  
15 20740, USA

16 <sup>5</sup>College of Global Change and Earth System Science, Beijing Normal University, Beijing,  
17 100875, China

18 <sup>6</sup>Key Laboratory for Cloud Physics, Chinese Academy of Meteorological Sciences, Beijing,  
19 100081, China

20 <sup>7</sup>Weather Modification Office of Hebei Province, Shijiazhuang, 050021, China

21 <sup>8</sup>School of Civil & Environmental Engineering, Georgia Institute of Technology, Atlanta, GA  
22 30332, USA

23 <sup>9</sup>College of Environmental Sciences and Engineering, Peking University, Beijing 100871, China

24

25

26 **Keywords:** Ozone Production Sensitivity, Airborne Measurements, OMI, CMAQ

27

28 Corresponding to Dr. Hao He ([haohe@umd.edu](mailto:haohe@umd.edu))

29

30 **Abstract**

31 To study the air pollution in the North China Plain (NCP), the Air Chemistry Research in  
32 Asia (ARIAs) campaign conducted airborne measurements of air pollutants including O<sub>3</sub>, CO,  
33 NO and NO<sub>2</sub> in spring 2016. High concentrations of pollutants, with maximum values >100  
34 ppbv of O<sub>3</sub>, >500 ppbv of CO, and >10 ppbv of NO<sub>2</sub>, were observed throughout the boundary  
35 layer during the campaign. CMAQ simulations with the 2010 EDGAR emissions can capture the  
36 basic spatial and temporal variations of ozone and its major precursors such as CO, NO<sub>x</sub> and  
37 VOCs, but significantly underestimate their concentrations. Observed emission enhancements of  
38 CO and NO<sub>x</sub> with respect to CO<sub>2</sub> suggest the existence of combustion with high emissions such  
39 as biomass burning in the NCP. The comparison with emission factors calculated from the 2010  
40 EDGAR emission inventory indicates that EDGAR overestimated the contribution of  
41 combustion with high emissions. Differences between CMAQ simulations with 2010 emissions  
42 and satellite observations in 2016 can reflect the change in anthropogenic emissions. NO<sub>x</sub>  
43 emissions decreased in megacities such as Beijing and Shanghai confirming the effectiveness of  
44 recent control measures in China, while in other cities and rural areas NO<sub>x</sub> emissions slightly  
45 increased, e.g., CMAQ predicts only ~81% of NO<sub>x</sub> observed in the aircraft campaign area.  
46 CMAQ also underestimates HCHO (a proxy of VOCs, by ~20%) and CO (by ~60%) over the  
47 NCP, suggesting adjustments of the 2010 EDGAR emissions are needed to improve the model  
48 performance. HCHO/NO<sub>2</sub> column ratios derived from OMI measurements and CMAQ  
49 simulations show that VOC-sensitive chemistry dominates the ozone photochemical production  
50 in eastern China, suggesting the importance of tightening regulations on VOCs emissions. After  
51 adjusting EDGAR emissions based on satellite observations, we conducted sensitivity  
52 experiments of CMAQ and achieved better model performance in simulating column contents of  
53 air pollutants. But CMAQ still underestimated air pollutant concentrations as compared with  
54 surface and aircraft observations. Because of the VOC-sensitive environment in ozone chemistry  
55 over the NCP, this study qualitatively suggested the underestimation of anthropogenic emissions  
56 could be important for CMAQ simulations while future study and regulations should focus on  
57 VOCs emissions with the continuous controls on NO<sub>x</sub> emissions in China.

58

## 59 **1. Introduction**

60 With rapid economic growth in the past three decades, the consumption of energy in  
61 China increased dramatically (Zhang and Cheng, 2009; Guan et al., 2018; Shan et al., 2018).  
62 Fossil fuels dominate total energy consumption, with coal still accounting for more than 50% of  
63 the carbon dioxide (CO<sub>2</sub>) emissions in China (Shan et al., 2018). This drastic increase in fossil  
64 fuel energy consumption is accompanied with deterioration of air quality (Chan and Yao, 2008;  
65 Fang et al., 2009), posing a threat to public health (Tie et al., 2009; Kan et al., 2012; Chen et al.,  
66 2013; Lelieveld et al., 2015). Particulate matter (PM) pollution, especially PM<sub>2.5</sub> in the North  
67 China Plain (NCP), drew public concern and governmental actions (He et al., 2001; Ye et al.,  
68 2003; Wang et al., 2005; Sun et al., 2006; Yang et al., 2011; Zhang et al., 2012; Zhang et al.,  
69 2013). PM pollution also has complex interactions with the planetary boundary layer (PBL) and  
70 its evolution, which can further degrade the air quality (Guo et al., 2016; Li et al., 2017b). Recent  
71 studies showed that tropospheric ozone (O<sub>3</sub>) pollution increased in China which exacerbated its  
72 complex air pollution problem (Xue et al., 2014; Verstraeten et al., 2015; Wang et al., 2017b; Ni  
73 et al., 2018).

74 Elevated ozone concentrations have adverse impacts on both human health (WHO, 2003;  
75 Anderson, 2009; Jerrett et al., 2009) and the ecosystem (Adams et al., 1989; Chameides et al.,  
76 1999; Ashmore, 2005). Tropospheric ozone absorbs thermal radiation and acts as the third most  
77 important anthropogenic contribution to radiative forcing of climate (Ramanathan and  
78 Dickinson, 1979; Lacis et al., 1990; IPCC, 2014). In the lower troposphere, the photolysis of  
79 ozone is an important source of atmospheric hydroxyl (OH) radicals that control the lifetimes of  
80 atmospheric species such as CO and volatile organic compounds (VOCs) (Logan et al., 1981;  
81 Thompson, 1992; Finlayson-Pitts and Pitts, 1999). Tropospheric ozone has a relatively long  
82 lifetime of several days to weeks (Stevenson et al., 2006; Young et al., 2013), leading to  
83 significant long-range transport of ozone and its precursors (Jacob et al., 1999; Derwent et al.,  
84 2004; Lin et al., 2008). Thus, investigation of ozone pollution in China is essential to support the  
85 national and international policy decision for air quality and the climate.

86 Tropospheric ozone is produced through complex photochemical reactions of precursors  
87 including nitrogen oxides (NO<sub>x</sub> = NO + NO<sub>2</sub>) and VOCs in the presence of sunlight  
88 (Haagensmit, 1952; Crutzen, 1974; Fishman et al., 1979; Seinfeld and Pandis, 2006). In China,

89 sectors of power generation, industry, and transportation dominates the NO<sub>x</sub> emissions (Streets et  
90 al., 2003; Ohara et al., 2007; Zhao et al., 2013a). Before 2010, NO<sub>x</sub> emissions in China increased  
91 substantially (Lin et al., 2010a; Zhao et al., 2013c). Analysis of satellite data revealed that  
92 recently NO<sub>x</sub> emissions have started decreasing in highly developed regions such as the Pearl  
93 River Delta (PRD), but still increased in other regions (Gu et al., 2013; Duncan et al., 2016; Liu  
94 et al., 2016). Anthropogenic VOCs emissions had a similar increasing trend in the past decades  
95 (Bo et al., 2008; Wei et al., 2011; Kurokawa et al., 2013; Zhao et al., 2017) and are projected to  
96 increase in the future (Zhang et al., 2018). Therefore the recent increase of tropospheric ozone in  
97 China could likely be explained by the enhanced anthropogenic emissions of ozone precursors.

98 Due to the complex O<sub>3</sub>-NO<sub>x</sub>-VOCs chemistry, we need to investigate the photochemical  
99 regime for local ozone production, i.e., NO<sub>x</sub>-sensitive or VOC-sensitive (Dodge, 1987;  
100 Kleinman, 1994). Duncan et al. (2010) used the ratio of tropospheric columns of formaldehyde  
101 (HCHO) and nitrogen dioxide (NO<sub>2</sub>) observed by the National Aeronautics and Space  
102 Administration (NASA) Aura Ozone Monitoring Instrument (OMI) to characterize ozone  
103 sensitivity. Studies show that a NO<sub>x</sub>-sensitive regime dominates in the United States, except in  
104 megacities such as Los Angeles and New York City where the local ozone production is in VOC-  
105 sensitive or in transition regimes (Duncan et al., 2010; Jin et al., 2017; Ring et al., 2018).  
106 However, VOC-sensitive and transition regimes for ozone photochemical production exist  
107 ubiquitously in China due to large amount of NO<sub>x</sub> emissions, especially over the NCP (Chou et  
108 al., 2009; Xing et al., 2011; Jin and Holloway, 2015; Jin et al., 2017). As such, although the  
109 current regulations in China focus only on reduction of NO<sub>x</sub> emissions (Wang and Hao, 2012;  
110 Wang et al., 2014a), air quality might also benefit from VOCs controls.

111 Aircraft measurements are essential to study the precursor emissions, photochemical  
112 production, and transport of ozone pollution at regional scale. However, airborne campaigns are  
113 sparse in China (Dickerson et al., 2007; Zhang et al., 2014; Ding et al., 2015; Huang et al., 2015;  
114 Wang et al., 2017a). To better understand the characteristics of ozone pollution, the Air  
115 Chemistry Research in Asia (ARIAs) aircraft campaign was conducted in Hebei Province of the  
116 NCP during May-June 2016, which was affiliated with the surface Aerosol Atmosphere  
117 Boundary-Layer Cloud (A<sup>2</sup>BC) experiment (Wang et al., 2018a; Wang et al., 2018b).  
118 Concentrations of major air pollutants in the lower atmosphere were measured during 11  
119 research flights in the NCP, which were conducted in association with the NASA Korea U.S. –

120 Air Quality (KORUS-AQ) campaign in downwind South Korea. Measurements collected in the  
121 ARIAs research flights and the A<sup>2</sup>BC surface observations provide a comprehensive dataset to  
122 thoroughly study the tropospheric ozone pollution and emissions of its precursors in China.

123 In this study, we evaluate anthropogenic emissions and the ozone pollution in the NCP  
124 using a combination of aircraft measurements, satellite observations, and modeling results. The  
125 U.S. Environmental Protection Agency (EPA) Community Multiscale Air Quality (CMAQ)  
126 model was used to simulate the atmospheric chemistry for the ARIAs campaign. We evaluate the  
127 emission data by comparing with the aircraft measurements and satellite products, and adjust  
128 emissions to improve the CMAQ performance. Lastly, we investigate the sensitivity of ozone  
129 production derived from CMAQ simulations and OMI observations and discuss the future ozone  
130 pollution in China.

131

## 132 **2. Data and Method**

### 133 **2.1 Aircraft campaign in the NCP**

134 With more than 250 million tons of iron and steel produced in 2016 (data from  
135 <http://data.stats.gov.cn>, accessed in September 2018), Hebei Province in the NCP is the most  
136 industrialized area in China. Due to its high emissions and proximity to megacities Beijing and  
137 Tianjin, the Beijing-Tianjin-Hebei area had severe air pollution in the past decade (Zhao et al.,  
138 2013b; Wang et al., 2014b). In May and June 2016, the ARIAs aircraft campaign was conducted  
139 over Hebei Province to investigate the emissions, chemical evolution, and transport of air  
140 pollutants. The airborne campaign was coordinated with the A<sup>2</sup>BC field campaign in Xingtai  
141 (XT, 37.18 °N, 114.36 °E, 182 m above sea level, ASL) and the NASA KORUS-AQ campaign to  
142 expand the study to East Asia. A Harbin Y12 research airplane (similar to the de Havilland Twin  
143 Otter) was employed to measure concentrations of air pollutants including O<sub>3</sub>, carbon monoxide  
144 (CO), CO<sub>2</sub>, NO<sub>2</sub>, and aerosol optical properties. The research airplane was located in Luancheng  
145 airport, hereafter referred to as LC (LC, 37.91 °N, 114.59 °E, 58 m ASL), south of Shijiazhuang,  
146 the capital city of Hebei province with 10 million population. Eleven research flights were  
147 conducted during the ARIAs campaign (Fig. S1 in the supplementary material). Vertical profiles  
148 of air pollutants from near surface (~100 m above ground level, AGL) to the free troposphere (>  
149 3000 m) were conducted over LC, XT (the supersite of the A<sup>2</sup>BC campaign), Julu (JL, 37.22 °N,

150 115.02 °E, 30 m ASL), and Quzhou (QZ, 36.76 °N, 114.96 °E, 40 m ASL).

151 The airborne measurements of ozone were conducted using a commercially available  
152 analyzer (Model 49C, Thermo Environmental Instruments, TEI, Franklin, Massachusetts)  
153 (Taubman et al., 2006). NO<sub>2</sub> was measured using a modified commercially available cavity ring-  
154 down spectroscopy (CRDS) detector (Castellanos et al., 2009; Brent et al., 2013). Nitrogen oxide  
155 (NO) and reactive nitrogen compounds (NO<sub>y</sub>) concentrations were analyzed using a commercial  
156 available NO analyzer (Model 42C, Thermo Environmental Instruments) with a hot molybdenum  
157 convertor working at 375 °C (Luke et al., 1992; Stehr et al., 2000). Ambient gas input was  
158 switched with and without the convertor frequently to measure NO and NO<sub>y</sub> simultaneous.  
159 However, due to high power demand of the instrument and convertor, NO and NO<sub>y</sub> were only  
160 measured during some research flights. Concentrations of CO and CO<sub>2</sub> were monitored with a 4-  
161 channel Picarro CRDS instrument (Model G2401-m, Picarro Inc., Santa Clara, CA), calibrated  
162 with CO/CO<sub>2</sub> standards certified at the National Institute of Standards and Technology (Ren et  
163 al., 2018). All the instruments were routinely serviced, calibrated and used for airborne  
164 measurements in the United States and China (Taubman et al., 2006; Dickerson et al., 2007;  
165 Hains et al., 2008; He et al., 2012; He et al., 2014; Ren et al., 2018; Salmon et al., 2018).  
166 Detailed information about the instrumentation including the sampling frequency, precisions and  
167 accuracies is listed in Tables S1 of the supplementary material. Measurements of ambient air  
168 pollutants were logged at 1 Hz frequency but the average times for different instruments are  
169 different as shown in Table S1. All measurements were synchronized based on the Picarro  
170 measurements of CO<sub>2</sub>, and CO with time, geolocation and altitude from the Global Position  
171 System (GPS). The delay and lag time of each instrument was considered during the post-  
172 processing of observation data and averaged to 1-min record for further analysis and model  
173 evaluation.

174 In the ARIAs research flights, 28 whole air samples (WAS) were collected in vertical  
175 spirals at different altitudes from ~400 m to ~3500 m. The WAS were analyzed using gas  
176 chromatography (GC) with Flame Ionization Detection (FID) and Mass Spectroscopy (MS) by  
177 the College of Environmental Sciences and Engineering at Peking University. 74 species of  
178 alkanes, alkenes/alkynes, aromatics, and halocarbons were identified and quantified for a study  
179 on ozone photochemical chemistry (see details in Benish et al., 2019). Detection limits for the  
180 compounds ranged from 2 to 50 pptv. Surface observation of trace gas pollutions including O<sub>3</sub>,

181 CO, NO, and NO<sub>x</sub> were measured at the A<sup>2</sup>BC Xingtai supersite using analyzers manufactured  
182 by Ecotech (Wang et al., 2018b); detailed description of the analyzers is discussed in Zhu et al.  
183 (2016). Surface HCHO concentrations were monitored using a formaldehyde analyzer (AERO  
184 LASER, Germany, Model 4021) based on fluorometric Hantzsch reactions (Gilpin et al., 1997;  
185 Rappenglück et al., 2010). All surface observations were collected as 1-min averaged data and  
186 processed to hourly mean values.

187

## 188 **2.2 Satellite products**

189 To evaluate the emissions and atmospheric chemistry in the NCP and greater East Asia,  
190 we used satellite observations of CO, NO<sub>2</sub>, and HCHO for May and June 2016. The  
191 Measurements of Pollution In the Troposphere (MOPITT) instrument onboard the NASA Terra  
192 satellite retrieved CO column contents with ~10:30 am local overpass time (Deeter et al., 2003).  
193 We used the latest version 7 MOPITT Level 3 daily gridded average products (1° × 1° spatial  
194 resolution, available at [https://eosweb.larc.nasa.gov/project/mopitt/mop03j\\_v007](https://eosweb.larc.nasa.gov/project/mopitt/mop03j_v007)) for the ARIAs  
195 campaign period (MOPITT Science Team, 2013). MOPITT thermal-infrared and near-infrared  
196 (TIR + NIR) products shows improved sensitivity to near surface CO in China (Worden et al.,  
197 2010). We used MOPITT near surface CO (~ 900 hPa) products and related averaging kernels  
198 (AKs) to evaluate the CMAQ results (Deeter et al., 2012).

199 OMI, onboard the NASA Aura satellite, is a UV/Vis solar backscatter spectrometer in a  
200 polar sun-synchronous orbit with a ~1:35 pm local overpass time. With high spatial resolution  
201 (13 km × 24 km for the center at nadir) and nearly daily coverage, OMI provided monitoring of  
202 trace gases and aerosol properties from 2005 (Levelt et al., 2006). The Version 3 OMI Level 2  
203 NO<sub>2</sub> products ([https://disc.gsfc.nasa.gov/datasets/OMNO2\\_V003/summary](https://disc.gsfc.nasa.gov/datasets/OMNO2_V003/summary)) (Krotkov et al.,  
204 2018) were used to evaluate the emissions and atmospheric chemistry in East Asia. Under clear  
205 sky, tropospheric NO<sub>2</sub> columns from OMI has precision of  $\sim 0.5 \times 10^{16}$  molecules cm<sup>-2</sup> and an  
206 accuracy of ±30% (Krotkov et al., 2017). OMI HCHO Version 3 Smithsonian Astronomical  
207 Observatory (SAO) ([https://disc.gsfc.nasa.gov/datasets/OMHCHO\\_V003/summary](https://disc.gsfc.nasa.gov/datasets/OMHCHO_V003/summary)) Level 2  
208 products were used in this study (Chance, 2007; González Abad et al., 2015). The precision of  
209 column HCHO is  $\sim 1.0 \times 10^{16}$  molecules cm<sup>-2</sup> and SAO products have an accuracy of ±25-30%  
210 without cloud (Millet et al., 2006; Boeke et al., 2011). Data in OMI pixels affected by the row  
211 anomaly and contaminated by clouds were filtered out using quality flags for both NO<sub>2</sub> and

212 HCHO columns.

213

### 214 **2.3 Model set-up**

215 We used CMAQ version 5.2 (EPA, 2017) to simulate atmospheric chemistry for the  
216 ARIAs campaign. The Weather Research and Forecasting (WRF) model Version 3.8.1  
217 (Skamarock et al., 2008) was driven by the European Centre for Medium-Range Weather  
218 Forecasts (ECMWF) ERA-Interim products (ds627.0, <https://rda.ucar.edu/datasets/ds627.0>) (Dee  
219 et al., 2011) to simulate meteorological fields. Two domains with spatial resolution of 36 km and  
220 12 km (Fig. 1) were used to cover East Asia, with 35 layers from the surface to 50 hPa and ~20  
221 layers in the lowest 2 km. Major physical options in WRF include the Rapid Radiative Transfer  
222 Model (RRTM) radiation scheme (Clough et al., 2005), the Pleim-Xiu surface layer and land  
223 surface model (Pleim and Xiu, 1995; Xiu and Pleim, 2001), the Asymmetric Convective Model  
224 (ACM2) boundary layer scheme (Pleim, 2007), the Kain-Fritsch cumulus scheme (Kain, 2004),  
225 and the WRF Single-Moment 6 (WSM-6) microphysics (Hong and Lim, 2006). The National  
226 Centers for Environmental Prediction (NCEP) ADP Global Surface and Upper Air Observational  
227 Weather Data (ds461.0 and ds351.0, <https://rda.ucar.edu>) were used to perform observational and  
228 analysis nudging on all domains following the method developed for NASA aircraft campaigns  
229 (He et al., 2014; Mazzuca et al., 2016). WRF outputs were processed by the EPA Meteorology-  
230 Chemistry Interface Processor Version 4.3 (MCIP v4.3, released in November 2015) for emission  
231 processing and CMAQ simulations.

232 Anthropogenic emissions were from the Emissions Database for Global Atmospheric  
233 Research Version 4.2 (EDGAR v4.2,  $0.1^\circ \times 0.1^\circ$  resolution) of year 2010, which are widely used  
234 for chemical transport modeling (European Commission, 2011). We used the EPA Sparse Matrix  
235 Operator Kernel Emissions (SMOKE) modeling system Version 4.5 (UNC, 2017) to project  
236 EDGAR emissions to the modeling domain. Emissions of air pollutants were speciated into  
237 Carbon Bond 05 chemical mechanism (Yarwood et al., 2005) and updated AERO6 aerosol  
238 module (Appel et al., 2013). The EDGAR v4.2 inventory has emissions for energy, industry,  
239 residential, and transport sectors. Without stack height information for power plants in the energy  
240 sector, we followed the approach developed in He et al. (2012) to locate these anthropogenic  
241 emissions at ~200 m above the surface as an approximation for averaged stack height and plume  
242 rise. We used the United States Geological Survey (USGS) 24 category land use dataset

243 combined with the Biogenic Emission Inventory System (BEIS) emission factors table to  
244 generate the input files for the CMAQ inline biogenic emissions modeling. Biogenic emissions  
245 were estimated using the BEIS module inline in CMAQ (EPA, 2017).

246 CMAQ v5.2 uses the updated Carbon Bond 6 (CB6r3) chemical mechanism (Yarwood et  
247 al., 2010) including improved chemistry mechanism for organic nitrates and peroxyacyl nitrates  
248 (PAN) chemistry and will lead to better performance for simulating Secondary Organic Aerosols  
249 (SOA) and tropospheric ozone in the United States (Appel et al., 2016). CMAQ was run with a  
250 coarse domain and a nested domain (Fig. 1). Chemical initial and boundary conditions for the  
251 coarse domain were obtained from the default concentration profiles built in CMAQ (EPA,  
252 2017). Results from the CMAQ coarse domain were used to generate boundary conditions for  
253 the nested domain. The WRF-CMAQ system was run from mid-April to June with the first 2  
254 weeks as spin-up. Hourly concentrations of air pollutants were saved for further analysis and  
255 model evaluation.

256

### 257 **3. Results and discussion**

#### 258 **3.1 Air Pollution in the NCP and CMAQ performance**

259 Figure 2 summarizes all aircraft measurements of O<sub>3</sub>, NO<sub>2</sub>, CO, and CO<sub>2</sub> over the NCP  
260 from eleven research flights. Generally, we observed high concentrations of air pollutants, with  
261 maximum values as >100 part per billion by volume (ppbv) of O<sub>3</sub>, >20 ppbv of NO<sub>2</sub>, >500 ppbv  
262 of CO, and >450 part per million by volume (ppmv) of CO<sub>2</sub>, in the aircraft campaign area  
263 (defined as 36.5-38.5°N, 114.0-115.5°E hereafter). We conducted vertical spirals over XT (the  
264 A<sup>2</sup>BC supersite), LC (the airport in south of Shijiazhuang), and two rural areas (JL and QZ)  
265 during the ARIAs research flights. Figure 3a summarizes vertical distributions and the mean  
266 profiles of air pollutants over XT, with mean O<sub>3</sub> concentrations of 80 ppbv in the lower  
267 atmosphere. We observed isolated plumes with >10 ppbv of NO<sub>2</sub>, >1000 ppbv of CO, and >440  
268 ppmv of CO<sub>2</sub> over XT, usually with a secondary maximum between 800 and 1200 m (a sample  
269 plume was presented in Fig. S2 of the supplementary material). These plumes aloft can play an  
270 important role in long-range transport of air pollutants to downwind regions. Profiles over LC  
271 (Fig. 3b) show higher O<sub>3</sub> concentrations (>100 ppbv) and relatively moderate NO<sub>2</sub> (~3 ppbv) and  
272 CO (~250 ppbv). The rural areas, JL and QZ, have relatively clean environment with <80 ppbv

273 of O<sub>3</sub>, <2 ppbv of NO<sub>2</sub>, and <300 ppbv of CO (Fig. 3c and 3d). Even the concentrations of air  
274 pollutants over the rural region in the NCP are comparable or higher than values in urban areas in  
275 North America and Europe. In summary, we found both south-north gradient and east-west  
276 gradient of air pollution in the campaign region, i.e., higher concentrations of air pollutants in the  
277 west XT-LC corridor near the mountain as compared with east side of JL and QZ, and higher  
278 concentrations in the north LC as compared with the south XT. Thus, the ARIAs research flights  
279 have good coverage of regions with both high and moderate concentrations of air pollutants and  
280 can fairly represent the regional nature of air pollution over the NCP.

281         Comparison of the surface trace gas observations at the Xingtai supersite and the CMAQ  
282 simulations driven by the EDGAR inventory (named baseline CMAQ case hereafter) reveals that  
283 CMAQ generally underestimates concentrations of major air pollutants (Fig. S3 in the  
284 supplementary material). The baseline CMAQ run successfully captures the diurnal and daily  
285 variations of surface ozone in Xingtai, although consistently underpredicts its concentrations. For  
286 CO and NO<sub>x</sub>, two important ozone precursors, CMAQ substantially underestimates their  
287 concentrations in Xingtai by more than 50% and especially fails to capture the extremely high  
288 values such as 6~7 ppmv of CO and ~100 ppbv of NO<sub>x</sub>. This underestimation could be caused by  
289 local sources poorly represented in the 12-km model simulations. For ambient HCHO, an  
290 important byproduct of VOC oxidization in ozone photochemical production, the baseline  
291 CMAQ run captures the variations, but substantially underestimates its concentrations. These  
292 results suggest that the underestimation of ozone precursors in CMAQ could lead to the poor  
293 model performance of simulating tropospheric ozone and other pollutants. It is worth noting that  
294 PBL dynamics could also play an important role in accurately simulating the concentrations of  
295 air pollutants, especially with the complex terrain at the Xingtai supersite (Figure S4 in the  
296 supplementary material). However, evaluation of the PBL simulations and advections in CMAQ  
297 is beyond the scope of this study, and we focus on the photochemistry of ozone here.

298         Similar analyses were conducted to investigate air pollutant concentrations in the lower  
299 troposphere over the NCP observed by the aircraft. A case of the research flight on June 11, 2016  
300 (Fig. S5 in the supplementary material) shows that CMAQ well captures the vertical gradient of  
301 air pollutants, while substantially underestimates concentrations of all trace gases except NO<sub>y</sub>.  
302 Since CMAQ generated hourly outputs, to alleviate the uncertainty of comparing 1-min aircraft  
303 data and hourly model simulations, we used 10-min averaged aircraft measurements which were

304 matched to the closest hourly model output following the approach described in Goldberg et al.  
305 (2016). Figure 4 shows similar underestimation (50% to 75% for all air pollutants) as compared  
306 with surface measurements (Fig. S3 in the supplementary material). CMAQ overestimates  $\text{NO}_y$   
307 but substantially underestimates NO and  $\text{NO}_2$ , which suggests that a significant amount of  
308 reactive nitrogen compounds could exist in the format of organic nitrates or nitrate aerosols in  
309 the model. Figure 5 compares total VOCs concentrations from WAS samples and CMAQ  
310 simulations, indicating that VOCs levels are also significantly underestimated by 80%. The  
311 model evaluation with surface and aircraft measurements suggest that ozone pollution in the  
312 NCP has been significantly underestimated in the baseline CMAQ run, which could be due to the  
313 uncertainty introduced by using the 2010 EDGAR emissions to simulate the 2016 ARIAs  
314 campaign period. Thus, we need to evaluate the emissions inventory data to improve the CMAQ  
315 performance and investigate the sensitivity of ozone production.

316

### 317 **3.2 Evaluation of emissions inventory in the NCP**

318 The EDGAR v4.2 emission inventory in East Asia was created based on the 2010 MIX  
319 emission inventory (Li et al., 2017a), so substantial changes were anticipated when used for the  
320 ARIAs campaign in 2016. Anthropogenic emission inventories are usually based on the “bottom-  
321 up” approach, which relies on the statistics of fossil fuel usage and emission factors (EFs) for  
322 each sector defined as the ratio of the amount of air pollutants released by a unit of  $\text{CO}_2$   
323 emissions, e.g.  $\text{CO}/\text{CO}_2$  and  $\text{NO}_x/\text{CO}_2$ . The 2010 EDGAR inventory has emissions for 4 sectors:  
324 Energy, Industry, Transportation, and Residential. We calculated the  $\text{CO}/\text{CO}_2$ ,  $\text{NO}_x/\text{CO}_2$ , and  
325  $\text{NO}_x/\text{CO}$  ratios through averaging the EFs from these 4 sectors (Fig. 6).

326 To evaluate the emission inventory data in the NCP, we used a plume recognition method  
327 to calculate the emission enhancements (EEs) from Y12 observations. We first selected 60 1-s  
328 aircraft measurements with a 60-s moving window. Then we conducted linear regression of  
329 observed air pollutant ( $\text{CO}$ ,  $\text{NO}_x$ , etc.) concentrations vs.  $\text{CO}_2$  concentrations in each 60-s  
330 window and calculated the slope (i.e.  $\Delta\text{CO}/\Delta\text{CO}_2$  and  $\Delta\text{NO}_x/\Delta\text{CO}_2$ ) and correlation (R). The  
331 slope is defined as EEs in each window, standing for a ‘plume’ tested in the 60-s window. Lastly,  
332 we only selected EEs that are within the PBL (below 1.5 km AGL in this study) and statistically  
333 significant ( $R^2 > 0.6$ ), so the values of these selected EEs can act as a proxy of EFs in the air  
334 mass observed. The detailed information about this plume recognition method can be found in

335 Halliday et al. (2019).

336 EEs observed during the research flights have a broad range of values.  $\Delta\text{CO}/\Delta\text{CO}_2$  ranges  
337 from below 1%, a typical value of modern automobile emissions, to higher than 10%, a value  
338 indicating fossil fuel combustion with high emissions such as biomass burning (Fig. 6a and 6b).  
339 The mean of observed EE for CO (3.7%) is close to that calculated from the EDGAR inventory  
340 (4.0%) in the aircraft campaign area. Observed  $\Delta\text{NO}_x/\Delta\text{CO}_2$  ratios also have isolated high values  
341 ( $>0.1\%$ ) with a mean value of 0.05%, which is substantially higher than the EF ( $\sim 0.03\%$ ) derived  
342 from the EDGAR inventory. Since estimation of anthropogenic  $\text{CO}_2$  flux in an urban/suburban  
343 area is challenging (Cambaliza et al., 2014; Heimbürger et al., 2017), the underestimation of CO  
344 and  $\text{NO}_x$  in the NCP could be caused by either underestimated EFs or uncertainty in  
345 anthropogenic  $\text{CO}_2$  emission data used in the ‘bottom-up’ approach.

346 To further investigate the characteristics of air pollutant emissions in the NCP, we  
347 conducted a similar analysis of  $\Delta\text{NO}_x/\Delta\text{CO}$ , which are usually co-emitted in combustion  
348 processes. Since around half of the CO and  $\text{NO}_x$  are from mobile sources in the EDGAR  
349 emission inventory, this ratio can approximately represent the emission characteristic of mobile  
350 sources in the NCP. The mean observed  $\Delta\text{NO}_x/\Delta\text{CO}$  ratio is  $\sim 1.3\%$ , significantly lower than  
351 5.6% based on the EDGAR emission inventory (Fig. 6c). These results suggest that the EDGAR  
352 emission inventory substantially overestimates the ratios of  $\text{NO}_x/\text{CO}$ , while the automobile  
353 emissions over the NCP in 2016 have been greatly improved due to recent regulations, i.e.,  
354 EDGAR overestimates the contribution from combustion with high emissions. It is worth noting  
355 that we only evaluated the emission ratios (EEs or EFs) in the EDGAR inventory, while the  
356 underestimation of CO and  $\text{NO}_x$  emissions could be caused by inaccurate  $\text{CO}_2$  emissions which  
357 have not been examined in this study.

358

### 359 **3.3 Evaluation of CO, $\text{NO}_x$ , and VOCs emissions using satellite data**

360 Satellite observations are widely used to evaluate the anthropogenic emissions in East  
361 Asia sometimes supplemented by model simulations, e.g., CO emissions using the MOPITT CO  
362 products (Jiang et al., 2015; Zheng et al., 2018), anthropogenic  $\text{NO}_x$  emissions using OMI  $\text{NO}_2$   
363 products (Wang et al., 2012; de Foy et al., 2015; Qu et al., 2017), and VOCs emissions using  
364 OMI HCHO products (Stavrakou et al., 2016). In this study, we used measurements from  
365 multiple satellite instruments to evaluate the CMAQ performance of  $\text{NO}_2$ , HCHO, and CO. Since

366 NO<sub>2</sub> and HCHO can be treated as proxy of NO<sub>x</sub> and VOCs emissions, we can further improve  
367 the 2010 EDGAR emissions over the NCP base on satellite data.

368 We followed the approach developed in Canty et al. (2015) to compare the tropospheric  
369 column contents of NO<sub>2</sub> from OMI products and CMAQ simulations. Level 2 OMI NO<sub>2</sub> swath  
370 information including row anomaly and quality flags were used to sample NO<sub>2</sub> vertical profiles  
371 from CMAQ outputs, and then CMAQ NO<sub>2</sub> column was calculated using the OMI averaging  
372 kernel (AK). Lastly, we averaged OMI and CMAQ NO<sub>2</sub> column contents to create daily 0.25° ×  
373 0.25° Level 3 products (see details in Canty et al., 2015). A similar approach was used to  
374 integrate HCHO column contents from CMAQ simulations based on OMI HCHO retrievals (see  
375 details in Ring et al., 2018) and construct daily 0.25° × 0.25° Level 3 HCHO products. For  
376 tropospheric CO, we selected the CO concentrations at ~ 900 hPa in CMAQ and averaged them  
377 to 1.0° × 1.0° daily products using MOPITT CO averaging kernel (MOPITT Science Team,  
378 2013). All gridded daily data of satellite and CMAQ were averaged in May and June 2016 for  
379 comparison.

380 Figure 7a shows strong signals over the NCP of the OMI NO<sub>2</sub> observations. We plotted  
381 OMI and CMAQ NO<sub>2</sub> columns over eastern China and the campaign area (Fig. 8). Generally,  
382 NO<sub>2</sub> columns from OMI and CMAQ agreed well over the eastern China (Fig. 8a) but large  
383 discrepancies with both overestimation and underestimation existed. For the aircraft campaign  
384 area, CMAQ underestimates NO<sub>2</sub> columns (slope = 0.95 and mean ratio = 0.81, i.e., only  
385 predicts 81% of OMI NO<sub>2</sub> column) with uncertainties relatively smaller within the 2-month  
386 period (Fig. 8b). However, in urban regions such as Beijing, the Yangtze River Delta (YRD), and  
387 the PRD, CMAQ substantially overestimates column NO<sub>2</sub> by up to 30%. Because the baseline  
388 CMAQ simulations used the 2010 anthropogenic emission data, these differences should reflect  
389 the changes in NO<sub>x</sub> emissions due to recent air pollution regulations. The comparison of NO<sub>2</sub>  
390 column suggests that NO<sub>x</sub> pollution of megacities in China has been substantially improved after  
391 2010 while NO<sub>x</sub> pollution in smaller cities and rural area has worsened, consistent with results  
392 from independent studies using OMI (Duncan et al., 2016; Krotkov et al., 2016). OMI HCHO  
393 retrievals also show high values over the NCP in spring when plants' photosynthetic activity is  
394 relatively low, reflecting that the domination of anthropogenic VOCs emissions in north China  
395 (Zhao et al., 2017). CMAQ has good agreement with OMI HCHO within the aircraft campaign  
396 area (<20% underestimation), but substantially underestimates HCHO columns in south China

397 where biogenic VOCs dominate (Fig. 7b). The MOPPIT products show high near-surface CO  
398 concentrations over the eastern China (Fig. 7c), while the baseline CMAQ run substantially  
399 underestimates CO concentrations over north China and only predicts 42% of the CO over the  
400 aircraft campaign area.

401 Using NO<sub>2</sub> and HCHO as proxies of NO<sub>x</sub> and VOCs emissions, the comparison of  
402 satellite observations and the baseline CMAQ simulations suggests that both NO<sub>x</sub> and VOCs  
403 emissions in the aircraft campaign area need to be adjusted for a better simulation of  
404 tropospheric ozone. Also the underestimation of CO, as an important precursor, can lead to  
405 underprediction of tropospheric ozone. We calculated the model/satellite ratios of NO<sub>x</sub>, HCHO,  
406 and CO in East Asia (Fig. S6 in the supplementary material) and used these ratios to adjust their  
407 anthropogenic emissions in CMAQ. The results will be discussed in Section 3.4.

408

### 409 **3.4 Tropospheric ozone production sensitivity from OMI and CMAQ**

410 Photochemical production of tropospheric ozone is highly non-linear and dependent on  
411 concentrations of NO<sub>x</sub> and VOCs (Kleinman, 1994; Sillman, 1999; Kleinman, 2000). A  
412 maximum rate of ozone production can be achieved with an optimal VOCs/NO<sub>x</sub> ratio. With other  
413 VOCs/NO<sub>x</sub> ratios, ozone production can be either in the VOC-sensitive regime (the rate of ozone  
414 production is controlled by VOCs concentrations) or in the NO<sub>x</sub>-sensitive regime (the rate of  
415 production is controlled by NO<sub>x</sub> concentrations). Different pollution control strategies can be  
416 implemented to reduce the tropospheric ozone levels in these two regimes. For instance, in a  
417 VOC-sensitive environment, reducing NO<sub>x</sub> emissions will lead to limited effects until the ozone  
418 production has been changed to a NO<sub>x</sub>-sensitive environment with the continuous remove of  
419 NO<sub>x</sub> from the atmosphere. Duncan et al. (2010) developed an approach using OMI HCHO/NO<sub>2</sub>  
420 column ratio to estimate the ozone production sensitivity as: 1) HCHO/NO<sub>2</sub> < 1: VOC-sensitive  
421 regime; 2) HCHO/NO<sub>2</sub> 1~2: transition regime; 3) HCHO/NO<sub>2</sub> > 2: NO<sub>x</sub>-sensitive regime.  
422 Studies show that urban areas in the U.S. such as Los Angeles, New York City and Houston are  
423 in VOC-sensitive or transition regimes, which lead to difficulty in local regulation of air quality  
424 (Duncan et al., 2010; Mazzuca et al., 2016; Ring et al., 2018). Recent studies suggest new  
425 threshold values of HCHO/NO<sub>2</sub> ratios between VOC-sensitive, transition, and NO<sub>x</sub>-sensitive  
426 regimes in the U.S. (Jin et al., 2017; Schroeder et al., 2017).

427 Using the Duncan et al. (2010) approach, studies using OMI products suggest large areas

428 of eastern China are either in VOC-sensitive regime (mostly megacities such as Beijing) or in  
429 transition regime (Jin and Holloway, 2015; Jin et al., 2017; Xing et al., 2018). We follow the  
430 approach described in Ring et al. (2018) to calculate the column HCHO/NO<sub>2</sub> ratios from OMI  
431 observations and CMAQ simulations for East Asia. OMI column HCHO/NO<sub>2</sub> ratios suggest that  
432 the ozone photochemical production is VOC-sensitive or in transition region over the NCP and  
433 other major urban areas such as YRD and PRD (Fig. 9a) if the Duncan et al. (2010) approach is  
434 applicable for these areas. CMAQ successfully captured the spatial distribution of the regional  
435 nature of ozone production sensitivity in eastern China, but predicted that the rate of ozone  
436 production is controlled more by VOCs with the CMAQ HCHO/NO<sub>2</sub> ratio lower than 1.0 in  
437 Beijing, YRD, and PRD (Fig. 9b). The VOC-sensitive environment from both OMI observations  
438 and CMAQ simulations suggests the rate of ozone photochemical production in the NCP is  
439 controlled not only by NO<sub>x</sub> emissions, but also by VOCs emissions which currently lack  
440 regulations in China. With continuous reduction of anthropogenic NO<sub>x</sub> emissions in China,  
441 VOCs controls might be efficient in these VOC-sensitive regions.

442

### 443 **3.5 Improvements of tropospheric ozone simulation using satellite products**

444 Results of the previous two sections show that the baseline CMAQ run substantially  
445 underestimates the concentrations of ozone and its major precursors in the NCP. Independent  
446 studies using KORUS-AQ observations and satellite products suggested that major ozone  
447 precursor emissions such as CO and NO<sub>x</sub> could have large discrepancies as compared with  
448 emission inventory in East Asia (Goldberg et al., 2019; Miyazaki et al., 2019). To identify the  
449 individual and combined effects of emission discrepancy of major ozone precursors in the NCP,  
450 we designed a series of sensitivity experiments with emissions adjusted to satellite observations.  
451 Unlike the top-down approach using global chemical transport models such GEOS-Chem (Lin et  
452 al., 2010b; Qu et al., 2017), here we simply applied the ratios of air pollutant column contents  
453 from satellite observations and CMAQ simulations on each 0.25 degree grids (Fig. S6 in the  
454 supplementary material) as:  $CO_{CMAQ}/CO_{MOPITT}$ ,  $NO_{2CMAQ}/NO_{2OMI}$ , and  $HCHO_{CMAQ}/HCHO_{OMI}$   
455 ratios for anthropogenic CO, NO<sub>x</sub>, and VOCs emissions, respectively. To estimate the  
456 contribution from biogenic VOCs emissions, we conducted one more run with the in-line BEIS  
457 module turned off. Table 1 shows the emission adjustments for the five sensitivity experiments.  
458 CMAQ was run for the nested 12 km domain (D02) with the same meteorology, initial

459 conditions, and boundary conditions derived from the coarse domain simulations. We conducted  
460 a similar analysis of Figure 4 to investigate the discrepancy between satellite products and  
461 CMAQ simulations over the eastern China (Figure S7 in the supplementary material).  
462 CMAQ\_all run successfully reproduced the column NO<sub>2</sub> and near surface CO in eastern China  
463 and column HCHO in the NCP. In southern China where biogenic VOCs dominate, adjusting  
464 anthropogenic VOCs emissions showed limited improvements on column HCHO simulations.

465 Figure 10 presents the evaluation of surface observations with respect to two sensitivity  
466 experiments (CMAQ\_baseline and CMAQ\_all with difference with respect to observations are  
467 showed in Figure S8 of the supplementary material; comparison with all CMAQ runs are  
468 presented in Fig. S9 in the supplementary material). CMAQ still might not capture the extreme  
469 high values of surface O<sub>3</sub> and CO (Fig. 10a and 10b) and only improved the model simulations  
470 slightly. For instance, the maximum CO concentration from CMAQ simulations are ~1700 ppbv  
471 while surface observations have CO peaks higher than 6000 ppbv (Fig. 10b). The adjustments of  
472 the emission inventory have improved the model simulations of NO<sub>2</sub>/NO (Fig. 10c and 10d) and  
473 HCHO (Fig. 10e). During the ARIAs flights, we observed various sources of emissions in the  
474 aircraft campaign area such as small factories and biomass burning, which are not included in the  
475 EDGAR emission inventory. So the reason for the model underestimation could be that the  
476 spatial resolution (12 km) of the nested CMAQ domain cannot represent the detailed emissions  
477 and resolve the local air pollution hotspots. However it is worth noting that even our CMAQ  
478 system is still not capable to reproduce the surface air quality at Xingtai, the adjustments of  
479 EDGAR emissions based on satellite observations reduce the underestimation.

480 The ARIAs flights covered a large area (~10<sup>4</sup> km<sup>2</sup>) in Hebei Province, which represent  
481 the regional nature of air pollution over the NCP. A case comparison of CMAQ\_All case and  
482 Y12 measurements on June 11, 2016 (Fig. 11) shows better results in both concentrations and  
483 vertical gradient of air pollutants (compared with Fig. S5 in the supplementary material),  
484 indicating the effectiveness of improving the emission inventories based on satellite  
485 observations. Table 2 summarizes the model performance of CMAQ as compared with aircraft  
486 measurements and scatter plots for each CMAQ sensitivity experiment are showed in Figure S10  
487 of the supplementary material. The adjustments of the EDGAR emissions with satellite  
488 observations substantially improved simulations of ozone pollution, with the root mean square  
489 error (RSME) decreasing from 25.1 ppbv (the baseline case) to 21.2 ppbv (CMAQ\_All case) and

490 the mean ratio of CMAQ simulations to aircraft observations increasing from 0.75 to 0.82. The  
491 model performance of CO has also been improved, with the RMSE decreasing from 247.0 ppbv  
492 to 203.6 ppbv and the mean ratio increasing from 0.40 to 0.66. For nitrogen compounds  
493 including NO<sub>2</sub>, NO, and NO<sub>y</sub>, the adjustments of EDGAR emissions have small impacts on  
494 improving the CMAQ performance. The reason could be that the ozone photochemistry is  
495 mainly VOC-sensitive over the NCP, so the adjustments of NO<sub>x</sub> emissions have limited impacts  
496 close to sources.

497

#### 498 **4. Conclusions and Discussion**

499 The ARIAs campaign conducted aircraft measurements over the NCP and observed high  
500 concentrations of air pollutants including O<sub>3</sub>, CO, and nitrogen compounds. CMAQ simulations  
501 driven by the 2010 EDGAR emissions substantially underestimate the levels of ozone and its  
502 precursors in the campaign region. Analysis of emission enhancements of CO and NO<sub>x</sub> with  
503 respect to concurrent CO<sub>2</sub> measurements suggests that the usage of the 2010 EDGAR emissions  
504 for the 2016 ARIAs campaign could introduce substantial uncertainty due to the recent changes  
505 of anthropogenic emissions in China. Comparison of atmospheric columns of NO<sub>2</sub> from CMAQ  
506 simulations and satellite observations suggests that NO<sub>x</sub> emissions decreased in megacities such  
507 as Beijing and Shanghai but increased in rural areas from 2010 to 2016. Similar analysis of  
508 HCHO and CO shows that the EDGAR VOCs and CO emissions could be also underestimated  
509 in the NCP. HCHO/NO<sub>2</sub> column ratio from OMI observations indicates tropospheric ozone  
510 production is mainly in the VOC-sensitive regime in the NCP, which is also confirmed by  
511 CMAQ simulations. To improve the model performance, we adjusted the EDGAR emissions  
512 over East Asia based on satellite observations. Better performance of simulating ozone and its  
513 precursors was achieved, while underestimation still exists.

514 Both satellite observations and CMAQ simulations indicate that the VOC-sensitive  
515 chemistry dominates the ozone photochemical production in eastern China, so the rate of local  
516 ozone production is mainly controlled by the VOCs emissions. In the past few years, despite  
517 implementation of control measures mainly on SO<sub>2</sub> and NO<sub>x</sub>, ozone concentrations have  
518 increased in China. Our study indicated that high NO<sub>x</sub> concentrations were pervasive in the PBL  
519 over rural areas of the NCP, where anthropogenic VOCs were also abundant. Reducing NO<sub>x</sub>

520 emissions is essential to control ozone on the regional scale, but our model simulations indicated  
521 that reducing VOCs emissions can lower the rate of photochemical smog production.

522 Currently, studies and regulations on anthropogenic VOCs emissions in China are  
523 lacking, so with expectation of further decreasing NO<sub>x</sub> emissions in China, more severe ozone  
524 pollution could be anticipated. It is worth noting that even VOCs controls can have beneficial  
525 impact on the local rate of ozone production in the VOC-sensitive regime, the ozone levels will  
526 not decrease until NO<sub>x</sub> emissions are substantially lower, i.e., regulations on VOCs are needed as  
527 well as the continuous controls on NO<sub>x</sub> emissions in China. These results can also partially  
528 explain why ozone pollution emerged in the past few years while PM<sub>2.5</sub> pollution has been  
529 substantially improved with strict regulations on anthropogenic emissions. New datasets such as  
530 the updated ‘bottom-up’ emissions inventory for East Asia and high resolution satellite  
531 observations such as TROPOMI products are needed to improve the modeling of ozone pollution  
532 in China, which can provide scientific evidence for future national and international regulations  
533 on air quality.

534

#### 535 **Author contribution**

536 X.R., R.D., H.H. and Z.L. designed the aircraft campaign; H.H., X.R., F.W., X.D., and F.L.  
537 performed the research flights; Y.W., X.R., and T.Z. conducted the surface observations; H.H.,  
538 T.P., and Y.H. developed the modeling system; H.H., X.R., and S.B. analyzed the data; H.H.,  
539 X.R., S.B. and R.D wrote the paper

540

#### 541 **Acknowledgements**

542 This work was funded by the National Science Foundation of the United States (Grant 1558259).  
543 We thank all of the A<sup>2</sup>BC and ARIAs research team, especially the flight crew of Hebei Weather  
544 Modification Office’s Y12 airplane. The flight campaign was conducted in association with the  
545 NASA’s KORUS-AQ campaign.

546

#### 547 **References**

548 Adams, R. M., Glycer, J. D., Johnson, S. L., and McCarl, B. A.: A reassessment of the economic-effects of ozone on  
549 United-States agriculture, *Japca-the Journal of the Air & Waste Management Association*, 39, 960-968,  
550 1989.  
551 Anderson, H. R.: Air pollution and mortality: A history, *Atmospheric Environment*, 43, 142-152,  
552 10.1016/j.atmosenv.2008.09.026, 2009.  
553 Appel, K. W., Pouliot, G. A., Simon, H., Sarwar, G., Pye, H. O. T., Napelenok, S. L., Akhtar, F., and Roselle, S. J.:

554 Evaluation of dust and trace metal estimates from the Community Multiscale Air Quality (CMAQ) model  
555 version 5.0, *Geoscientific Model Development*, 6, 883-899, 10.5194/gmd-6-883-2013, 2013.

556 Appel, K. W., Napelenok, S. L., Hogrefe, C., Foley, K. M., Pouliot, G., Murphy, B. N., Luecken, D. J., and Heath,  
557 N.: Evaluation of the Community Multiscale Air Quality (CMAQ) Model Version 5.2, 2016 CMAS  
558 Conference, Chapel Hill, NC., 2016.

559 Ashmore, M. R.: Assessing the future global impacts of ozone on vegetation, *Plant Cell Environ.*, 28, 949-964,  
560 10.1111/j.1365-3040.2005.01341.x, 2005.

561 Benish, S. E., He, H., Ren, X., Roberts, S., Salawitch, R. J., Li, Z., Wang, F., Zhang, F., Wang, Y., Shao, M., Lu, S.,  
562 Pfister, G., Flocke, F., and Dickerson, R.: Observations of Nitrogen Oxides and Volatile Organic  
563 Compounds over the North China Plain and Impact on Ozone Formation, *Journal of Geophysical Research*,  
564 *undere review*, 2019.

565 Bo, Y., Cai, H., and Xie, S. D.: Spatial and temporal variation of historical anthropogenic NMVOCs emission  
566 inventories in China, *Atmospheric Chemistry and Physics*, 8, 7297-7316, 10.5194/acp-8-7297-2008, 2008.

567 Boeke, N. L., Marshall, J. D., Alvarez, S., Chance, K. V., Fried, A., Kurosu, T. P., Rappenglück, B., Richter, D.,  
568 Walega, J., Weibring, P., and Millet, D. B.: Formaldehyde columns from the Ozone Monitoring Instrument:  
569 Urban versus background levels and evaluation using aircraft data and a global model, *Journal of*  
570 *Geophysical Research: Atmospheres*, 116, doi:10.1029/2010JD014870, 2011.

571 Brent, L. C., Thorn, W. J., Gupta, M., Leen, B., Stehr, J. W., He, H., Arkinson, H. L., Weinheimer, A., Garland, C.,  
572 Pusede, S. E., Wooldridge, P. J., Cohen, R. C., and Dickerson, R. R.: Evaluation of the use of a  
573 commercially available cavity ringdown absorption spectrometer for measuring NO<sub>2</sub> in flight, and  
574 observations over the Mid-Atlantic States, during DISCOVER-AQ, *Journal of Atmospheric Chemistry*, 1-  
575 19, 10.1007/s10874-013-9265-6, 2013.

576 Cambaliza, M. O. L., Shepson, P. B., Caulton, D. R., Stirm, B., Samarov, D., Gurney, K. R., Turnbull, J., Davis, K.  
577 J., Possolo, A., Karion, A., Sweeney, C., Moser, B., Hendricks, A., Lauvaux, T., Mays, K., Whetstone, J.,  
578 Huang, J., Razlivanov, I., Miles, N. L., and Richardson, S. J.: Assessment of uncertainties of an aircraft-  
579 based mass balance approach for quantifying urban greenhouse gas emissions, *Atmospheric Chemistry and*  
580 *Physics*, 14, 9029-9050, 10.5194/acp-14-9029-2014, 2014.

581 Canty, T. P., Hembeck, L., Vinciguerra, T. P., Anderson, D. C., Goldberg, D. L., Carpenter, S. F., Allen, D. J.,  
582 Loughner, C. P., Salawitch, R. J., and Dickerson, R. R.: Ozone and NO<sub>x</sub> chemistry in the eastern US:  
583 evaluation of CMAQ/CB05 with satellite (OMI) data, *Atmospheric Chemistry and Physics*, 15, 10965-  
584 10982, 10.5194/acp-15-10965-2015, 2015.

585 Castellanos, P., Luke, W. T., Kelley, P., Stehr, J. W., Ehrman, S. H., and Dickerson, R. R.: Modification of a  
586 commercial cavity ring-down spectroscopy NO<sub>2</sub> detector for enhanced sensitivity, *Review of Scientific*  
587 *Instruments*, 80, 113107, 10.1063/1.3244090, 2009.

588 Chameides, W. L., Li, X. S., Tang, X. Y., Zhou, X. J., Luo, C., Kiang, C. S., St John, J., Saylor, R. D., Liu, S. C.,  
589 Lam, K. S., Wang, T., and Giorgi, F.: Is ozone pollution affecting crop yields in China?, *Geophysical*  
590 *Research Letters*, 26, 867-870, 10.1029/1999gl1900068, 1999.

591 Chan, C. K., and Yao, X.: Air pollution in mega cities in China, *Atmospheric Environment*, 42, 1-42,  
592 10.1016/j.atmosenv.2007.09.003, 2008.

593 Chance, K.: OMI/Aura Formaldehyde (HCHO) Total Column 1-orbit L2 Swath 13x24 km V003, Greenbelt, MD,  
594 USA, Goddard Earth Sciences Data and Information Services Center (GES DISC), Accessed: January  
595 2018, 10.5067/Aura/OMI/DATA2015, 2007.

596 Chen, Y. Y., Ebenstein, A., Greenstone, M., and Li, H. B.: Evidence on the impact of sustained exposure to air  
597 pollution on life expectancy from China's Huai River policy, *Proc. Natl. Acad. Sci. U. S. A.*, 110, 12936-  
598 12941, 10.1073/pnas.1300018110, 2013.

599 Chou, C. C. K., Tsai, C.-Y., Shiu, C.-J., Liu, S. C., and Zhu, T.: Measurement of NO<sub>y</sub> during Campaign of Air  
600 Quality Research in Beijing 2006 (CAREBeijing-2006): Implications for the ozone production efficiency of  
601 NO<sub>x</sub>, *Journal of Geophysical Research-Atmospheres*, 114, D00g01, 10.1029/2008jd010446, 2009.

602 Clough, S. A., Shephard, M. W., Mlawer, E. J., Delamere, J. S., Iacono, M. J., Cady-Pereira, K., Boukabara, S., and  
603 Brown, P. D.: Atmospheric radiative transfer modeling: a summary of the AER codes, *Journal of*  
604 *Quantitative Spectroscopy and Radiative Transfer*, 91, 233-244, <https://doi.org/10.1016/j.jqsrt.2004.05.058>,  
605 2005.

606 Crutzen, P. J.: Photochemical reactions initiated by and influencing ozone in unpolluted tropospheric air, *Tellus*, 26,  
607 47-57, 1974.

608 de Foy, B., Lu, Z., Streets, D. G., Lamsal, L. N., and Duncan, B. N.: Estimates of power plant NO<sub>x</sub> emissions and  
609 lifetimes from OMI NO<sub>2</sub> satellite retrievals, *Atmospheric Environment*, 116, 1-11,

610 <http://dx.doi.org/10.1016/j.atmosenv.2015.05.056>, 2015.

611 Dee, D. P., Uppala, S. M., Simmons, A. J., Berrisford, P., Poli, P., Kobayashi, S., Andrae, U., Balmaseda, M. A.,  
612 Balsamo, G., Bauer, P., Bechtold, P., Beljaars, A. C. M., van de Berg, L., Bidlot, J., Bormann, N., Delsol,  
613 C., Dragani, R., Fuentes, M., Geer, A. J., Haimberger, L., Healy, S. B., Hersbach, H., Hólm, E. V., Isaksen,  
614 L., Kållberg, P., Köhler, M., Matricardi, M., McNally, A. P., Monge-Sanz, B. M., Morcrette, J. J., Park, B.  
615 K., Peubey, C., de Rosnay, P., Tavolato, C., Thépaut, J. N., and Vitart, F.: The ERA-Interim reanalysis:  
616 configuration and performance of the data assimilation system, *Q. J. R. Meteorol. Soc.*, 137, 553-597,  
617 10.1002/qj.828, 2011.

618 Deeter, M. N., Emmons, L. K., Francis, G. L., Edwards, D. P., Gille, J. C., Warner, J. X., Khattatov, B., Ziskin, D.,  
619 Lamarque, J. F., Ho, S. P., Yudin, V., Attie, J. L., Packman, D., Chen, J., Mao, D., and Drummond, J. R.:  
620 Operational carbon monoxide retrieval algorithm and selected results for the MOPITT instrument, *Journal*  
621 *of Geophysical Research-Atmospheres*, 108, 4399, 10.1029/2002jd003186, 2003.

622 Deeter, M. N., Worden, H. M., Edwards, D. P., Gille, J. C., and Andrews, A. E.: Evaluation of MOPITT retrievals of  
623 lower-tropospheric carbon monoxide over the United States, *Journal of Geophysical Research-*  
624 *Atmospheres*, 117, D13306, 10.1029/2012jd017553, 2012.

625 Derwent, R. G., Stevenson, D. S., Collins, W. J., and Johnson, C. E.: Intercontinental transport and the origins of the  
626 ozone observed at surface sites in Europe, *Atmospheric Environment*, 38, 1891-1901,  
627 10.1016/j.atmosenv.2004.01.008, 2004.

628 Dickerson, R. R., Li, C., Li, Z., Marufu, L. T., Stehr, J. W., McClure, B., Krotkov, N., Chen, H., Wang, P., Xia, X.,  
629 Ban, X., Gong, F., Yuan, J., and Yang, J.: Aircraft observations of dust and pollutants over northeast China:  
630 Insight into the meteorological mechanisms of transport, *Journal of Geophysical Research-Atmospheres*,  
631 112, D24s90, 10.1029/2007jd008999, 2007.

632 Ding, K., Liu, J., Ding, A., Liu, Q., Zhao, T. L., Shi, J., Han, Y., Wang, H., and Jiang, F.: Uplifting of carbon  
633 monoxide from biomass burning and anthropogenic sources to the free troposphere in East Asia,  
634 *Atmospheric Chemistry and Physics*, 15, 2843-2866, 10.5194/acp-15-2843-2015, 2015.

635 Dodge, M.: *Chemistry of Oxidant Formation: Implications for Designing Effective Control Strategies U.S.*  
636 *Environmental Protection Agency, Washington, D.C. EPA/600/D-87/114 (NTIS PB87179990)*, 1987.

637 Duncan, B. N., Yoshida, Y., Olson, J. R., Sillman, S., Martin, R. V., Lamsal, L., Hu, Y. T., Pickering, K. E., Retscher,  
638 C., Allen, D. J., and Crawford, J. H.: Application of OMI observations to a space-based indicator of NO<sub>x</sub>  
639 and VOC controls on surface ozone formation, *Atmospheric Environment*, 44, 2213-2223,  
640 10.1016/j.atmosenv.2010.03.010, 2010.

641 Duncan, B. N., Lamsal, L. N., Thompson, A. M., Yoshida, Y., Lu, Z. F., Streets, D. G., Hurwitz, M. M., and  
642 Pickering, K. E.: A space-based, high-resolution view of notable changes in urban NO<sub>x</sub> pollution around  
643 the world (2005-2014), *Journal of Geophysical Research-Atmospheres*, 121, 976-996,  
644 10.1002/2015jd024121, 2016.

645 EPA: CMAQ (Version 5.2) Scientific Document, Zenodo. <http://doi.org/10.5281/zenodo.1167892>, 2017.

646 European Commission: Joint Research Centre (JRC)/Netherlands Environmental Assessment Agency (PBL).  
647 Emission Database for Global Atmospheric Research (EDGAR), release version 4.2., available at:  
648 <http://edgar.jrc.ec.europa.eu> (accessed in March 2017), 2011.

649 Fang, M., Chan, C. K., and Yao, X. H.: Managing air quality in a rapidly developing nation: China, *Atmospheric*  
650 *Environment*, 43, 79-86, 10.1016/j.atmosenv.2008.09.064, 2009.

651 Finlayson-Pitts, B. J., and Pitts, J. N.: *Chemistry of the Upper and Lower Atmosphere*, 1st ed., Academic Press, UK,  
652 1999.

653 Fishman, J., Solomon, S., and Crutzen, P. J.: Observational and theoretical evidence in support of a significant insitu  
654 photo-chemical source of tropospheric ozone, *Tellus*, 31, 432-446, 1979.

655 Gilpin, T., Apel, E., Fried, A., Wert, B., Calvert, J., Genfa, Z., Dasgupta, P., Harder, J. W., Heikes, B., Hopkins, B.,  
656 Westberg, H., Kleindienst, T., Lee, Y.-N., Zhou, X., Lonneman, W., and Sewell, S.: Intercomparison of six  
657 ambient [CH<sub>2</sub>O] measurement techniques, *Journal of Geophysical Research: Atmospheres*, 102, 21161-  
658 21188, 10.1029/97jd01314, 1997.

659 Goldberg, D. L., Vinciguerra, T. P., Anderson, D. C., Hembeck, L., Canty, T. P., Ehrman, S. H., Martins, D. K.,  
660 Stauffer, R. M., Thompson, A. M., Salawitch, R. J., and Dickerson, R. R.: CAMx Ozone Source Attribution  
661 in the Eastern United States using Guidance from Observations during DISCOVER-AQ Maryland,  
662 *Geophysical Research Letters*, 2015GL067332, 10.1002/2015gl067332, 2016.

663 Goldberg, D. L., Saide, P. E., Lamsal, L. N., de Foy, B., Lu, Z., Woo, J. H., Kim, Y., Kim, J., Gao, M., Carmichael,  
664 G., and Streets, D. G.: A top-down assessment using OMI NO<sub>2</sub> suggests an underestimate in the NO<sub>x</sub>  
665 emissions inventory in Seoul, South Korea, during KORUS-AQ, *Atmos. Chem. Phys.*, 19, 1801-1818,

666 10.5194/acp-19-1801-2019, 2019.

667 González Abad, G., Liu, X., Chance, K., Wang, H., Kurosu, T. P., and Suleiman, R.: Updated Smithsonian  
668 Astrophysical Observatory Ozone Monitoring Instrument (SAO OMI) formaldehyde retrieval, *Atmos.*  
669 *Meas. Tech.*, 8, 19-32, 10.5194/amt-8-19-2015, 2015.

670 Gu, D. S., Wang, Y. H., Smeltzer, C., and Liu, Z.: Reduction in NO<sub>x</sub> Emission Trends over China: Regional and  
671 Seasonal Variations, *Environmental Science & Technology*, 47, 12912-12919, 10.1021/es401727e, 2013.

672 Guan, D. B., Meng, J., Reiner, D. M., Zhang, N., Shan, Y. L., Mi, Z. F., Shao, S., Liu, Z., Zhang, Q., and Davis, S. J.:  
673 Structural decline in China's CO<sub>2</sub> emissions through transitions in industry and energy systems, *Nature*  
674 *Geoscience*, 11, 551+, 10.1038/s41561-018-0161-1, 2018.

675 Guo, J., Miao, Y., Zhang, Y., Liu, H., Li, Z., Zhang, W., He, J., Lou, M., Yan, Y., Bian, L., and Zhai, P.: The  
676 climatology of planetary boundary layer height in China derived from radiosonde and reanalysis data,  
677 *Atmos. Chem. Phys.*, 16, 13309-13319, 10.5194/acp-16-13309-2016, 2016.

678 Haagensmit, A. J.: Chemistry and physiology of Los-Angeles smog, *Industrial and Engineering Chemistry*, 44,  
679 1342-1346, 10.1021/ie50510a045, 1952.

680 Hains, J. C., Taubman, B. F., Thompson, A. M., Stehr, J. W., Marufu, L. T., Doddridge, B. G., and Dickerson, R. R.:  
681 Origins of chemical pollution derived from Mid-Atlantic aircraft profiles using a clustering technique,  
682 *Atmospheric Environment*, 42, 1727-1741, 10.1016/j.atmosenv.2007.11.052, 2008.

683 Halliday, H. S., DiGangi, J. P., Choi, Y., Diskin, G. S., Pusede, S. E., Rana, M., Nowak, J. B., Knote, C., Ren, X.,  
684 He, H., Dickerson, R. R., and Li, Z.: Using Short-Term CO/CO<sub>2</sub> Ratios to Assess Air Mass Differences  
685 over the Korean Peninsula during KORUS-AQ, *Journal of Geophysical Research: Atmospheres*, 0,  
686 10.1029/2018jd029697, 2019.

687 He, H., Li, C., Loughner, C. P., Li, Z., Krotkov, N. A., Yang, K., Wang, L., Zheng, Y., Bao, X., Zhao, G., and  
688 Dickerson, R. R.: SO<sub>2</sub> over central China: Measurements, numerical simulations and the tropospheric  
689 sulfur budget, *Journal of Geophysical Research: Atmospheres*, 117, doi:10.1029/2011JD016473, 2012.

690 He, H., Loughner, C. P., Stehr, J. W., Arkinson, H. L., Brent, L. C., Follette-Cook, M. B., Tzortziou, M. A.,  
691 Pickering, K. E., Thompson, A. M., Martins, D. K., Diskin, G. S., Anderson, B. E., Crawford, J. H.,  
692 Weinheimer, A. J., Lee, P., Hains, J. C., and Dickerson, R. R.: An elevated reservoir of air pollutants over  
693 the Mid-Atlantic States during the 2011 DISCOVER-AQ campaign: Airborne measurements and numerical  
694 simulations, *Atmospheric Environment*, 85, 18-30, 10.1016/j.atmosenv.2013.11.039, 2014.

695 He, K. B., Yang, F. M., Ma, Y. L., Zhang, Q., Yao, X. H., Chan, C. K., Cadle, S., Chan, T., and Mulawa, P.: The  
696 characteristics of PM<sub>2.5</sub> in Beijing, China, *Atmospheric Environment*, 35, 4959-4970, 10.1016/s1352-  
697 2310(01)00301-6, 2001.

698 Heimbürger, A. M. F., Harvey, R. M., Shepson, P. B., Stirm, B. H., Gore, C., Turnbull, J., Cambaliza, M. O. L.,  
699 Salmon, O. E., Kerlo, A. E. M., Lavoie, T. N., Davis, K. J., Lauvaux, T., Karion, A., Sweeney, C., Brewer,  
700 W. A., Hardesty, R. M., and Gurney, K. R.: Assessing the optimized precision of the aircraft mass balance  
701 method for measurement of urban greenhouse gas emission rates through averaging, *Elementa-Science of*  
702 *the Anthropocene*, 5, 26, 10.1525/elementa.134, 2017.

703 Hong, S.-Y., and Lim, J.-O.: The WRF single-moment 6-class microphysics scheme (WSM6), *J. Korean Meteor.*  
704 *Soc.*, 42, 129-151, 2006.

705 Huang, J., Liu, H., Crawford, J. H., Chan, C., Considine, D. B., Zhang, Y., Zheng, X., Zhao, C., Thouret, V.,  
706 Oltmans, S. J., Liu, S. C., Jones, D. B. A., Steenrod, S. D., and Damon, M. R.: Origin of springtime ozone  
707 enhancements in the lower troposphere over Beijing: in situ measurements and model analysis,  
708 *Atmospheric Chemistry and Physics*, 15, 5161-5179, 10.5194/acp-15-5161-2015, 2015.

709 IPCC: Climate Change 2014: Synthesis Report. Contribution of Working Groups I, II and III to the Fifth Assessment  
710 Report of the Intergovernmental Panel on Climate Change [Core Writing Team, R.K. Pachauri and L.A.  
711 Meyer (eds.)], IPCC, Geneva, Switzerland, 151 pp., 2014.

712 Jacob, D. J., Logan, J. A., and Murti, P. P.: Effect of rising Asian emissions on surface ozone in the United States,  
713 *Geophysical Research Letters*, 26, 2175-2178, 10.1029/1999gl900450, 1999.

714 Jerrett, M., Burnett, R. T., Pope, C. A., Ito, K., Thurston, G., Krewski, D., Shi, Y. L., Calle, E., and Thun, M.: Long-  
715 Term Ozone Exposure and Mortality, *N. Engl. J. Med.*, 360, 1085-1095, 10.1056/NEJMoa0803894, 2009.

716 Jiang, Z., Worden, J. R., Jones, D. B. A., Lin, J. T., Verstraeten, W. W., and Henze, D. K.: Constraints on Asian  
717 ozone using Aura TES, OMI and Terra MOPITT, *Atmospheric Chemistry and Physics*, 15, 99-112,  
718 10.5194/acp-15-99-2015, 2015.

719 Jin, X., and Holloway, T.: Spatial and temporal variability of ozone sensitivity over China observed from the Ozone  
720 Monitoring Instrument, *Journal of Geophysical Research: Atmospheres*, 120, 7229-7246,  
721 doi:10.1002/2015JD023250, 2015.

722 Jin, X., Fiore, A. M., Murray, L. T., Valin, L. C., Lamsal, L. N., Duncan, B., Folkert Boersma, K., De Smedt, I.,  
723 Abad, G. G., Chance, K., and Tonnesen, G. S.: Evaluating a Space-Based Indicator of Surface Ozone-NOx-  
724 VOC Sensitivity Over Midlatitude Source Regions and Application to Decadal Trends, *Journal of*  
725 *Geophysical Research: Atmospheres*, 122, 10,439-410,461, doi:10.1002/2017JD026720, 2017.

726 Kain, J. S.: The Kain-Fritsch convective parameterization: An update, *Journal of Applied Meteorology*, 43, 170-181,  
727 2004.

728 Kan, H. D., Chen, R. J., and Tong, S. L.: Ambient air pollution, climate change, and population health in China,  
729 *Environ. Int.*, 42, 10-19, 10.1016/j.envint.2011.03.003, 2012.

730 Kleinman, L. I.: Low and high NOx tropospheric photochemistry, *Journal of Geophysical Research-Atmospheres*,  
731 99, 16831-16838, 10.1029/94jd01028, 1994.

732 Kleinman, L. I.: Ozone process insights from field experiments - part II: Observation-based analysis for ozone  
733 production, *Atmospheric Environment*, 34, 2023-2033, 10.1016/s1352-2310(99)00457-4, 2000.

734 Krotkov, N. A., McLinden, C. A., Li, C., Lamsal, L. N., Celarier, E. A., Marchenko, S. V., Swartz, W. H., Bucsela, E.  
735 J., Joiner, J., Duncan, B. N., Boersma, K. F., Veefkind, J. P., Levelt, P. F., Fioletov, V. E., Dickerson, R. R.,  
736 He, H., Lu, Z. F., and Streets, D. G.: Aura OMI observations of regional SO2 and NO2 pollution changes  
737 from 2005 to 2015, *Atmospheric Chemistry and Physics*, 16, 4605-4629, 10.5194/acp-16-4605-2016, 2016.

738 Krotkov, N. A., Lamsal, L. N., Celarier, E. A., Swartz, W. H., Marchenko, S. V., Bucsela, E. J., Chan, K. L., Wenig,  
739 M., and Zara, M.: The version 3 OMI NO2 standard product, *Atmos. Meas. Tech.*, 10, 3133-3149,  
740 10.5194/amt-10-3133-2017, 2017.

741 Krotkov, N. A., Lamsal, L. N., Marchenko, S. V., Celarier, E. A., bucsela, E. J., Swartz, W. H., and Veefkind, J. P.:  
742 OMI/Aura Nitrogen Dioxide (NO2) Total and Tropospheric Column 1-orbit L2 Swath 13x24 km V003,  
743 Greenbelt, MD, USA, Goddard Earth Sciences Data and Information Services Center (GES DISC),  
744 Accessed: January 2018, 10.5067/Aura/OMI/DATA2017, 2018.

745 Kurokawa, J., Ohara, T., Morikawa, T., Hanayama, S., Janssens-Maenhout, G., Fukui, T., Kawashima, K., and  
746 Akimoto, H.: Emissions of air pollutants and greenhouse gases over Asian regions during 2000-2008:  
747 Regional Emission inventory in ASia (REAS) version 2, *Atmospheric Chemistry and Physics*, 13, 11019-  
748 11058, 10.5194/acp-13-11019-2013, 2013.

749 Lacis, A. A., Wuebbles, D. J., and Logan, J. A.: Radiative forcing of climate by changes in the vertical-distribution  
750 of ozone, *Journal of Geophysical Research-Atmospheres*, 95, 9971-9981, 10.1029/JD095iD07p09971,  
751 1990.

752 Lelieveld, J., Evans, J. S., Fnais, M., Giannadaki, D., and Pozzer, A.: The contribution of outdoor air pollution  
753 sources to premature mortality on a global scale, *Nature*, 525, 367-+, 10.1038/nature15371, 2015.

754 Levelt, P. F., Hilsenrath, E., Leppelmeier, G. W., van den Oord, G. H. J., Bhartia, P. K., Tamminen, J., de Haan, J. F.,  
755 and Veefkind, J. P.: Science objectives of the Ozone Monitoring Instrument, *Ieee Transactions on*  
756 *Geoscience and Remote Sensing*, 44, 1199-1208, 10.1109/tgrs.2006.872336, 2006.

757 Li, M., Zhang, Q., Kurokawa, J., Woo, J. H., He, K. B., Lu, Z. F., Ohara, T., Song, Y., Streets, D. G., Carmichael, G.  
758 R., Cheng, Y. F., Hong, C. P., Huo, H., Jiang, X. J., Kang, S. C., Liu, F., Su, H., and Zheng, B.: MIX: a  
759 mosaic Asian anthropogenic emission inventory under the international collaboration framework of the  
760 MICS-Asia and HTAP, *Atmospheric Chemistry and Physics*, 17, 935-963, 10.5194/acp-17-935-2017,  
761 2017a.

762 Li, Z., Guo, J., Ding, A., Liao, H., Liu, J., Sun, Y., Wang, T., Xue, H., Zhang, H., and Zhu, B.: Aerosol and  
763 boundary-layer interactions and impact on air quality, *National Science Review*, 4, 810-833,  
764 10.1093/nsr/nwx117, 2017b.

765 Lin, J., Nielsen, C. P., Zhao, Y., Lei, Y., Liu, Y., and McElroy, M. B.: Recent Changes in Particulate Air Pollution  
766 over China Observed from Space and the Ground: Effectiveness of Emission Control, *Environmental*  
767 *Science & Technology*, 44, 7771-7776, 10.1021/es101094t, 2010a.

768 Lin, J. T., Wuebbles, D. J., and Liang, X. Z.: Effects of intercontinental transport on surface ozone over the United  
769 States: Present and future assessment with a global model, *Geophysical Research Letters*, 35, L02805,  
770 10.1029/2007gl031415, 2008.

771 Lin, J. T., McElroy, M. B., and Boersma, K. F.: Constraint of anthropogenic NOx emissions in China from different  
772 sectors: a new methodology using multiple satellite retrievals, *Atmospheric Chemistry and Physics*, 10, 63-  
773 78, 10.5194/acp-10-63-2010, 2010b.

774 Liu, F., Zhang, Q., Ronald, J. V., Zheng, B., Tong, D., Yan, L., Zheng, Y. X., and He, K. B.: Recent reduction in NOx  
775 emissions over China: synthesis of satellite observations and emission inventories, *Environ. Res. Lett.*, 11,  
776 114002, 10.1088/1748-9326/11/11/114002, 2016.

777 Logan, J. A., Prather, M. J., Wofsy, S. C., and McElroy, M. B.: Tropospheric chemistry - a global perspective,

778 Journal of Geophysical Research-Oceans and Atmospheres, 86, 7210-7254, 10.1029/JC086iC08p07210,  
779 1981.

780 Luke, W. T., Dickerson, R. R., Ryan, W. F., Pickering, K. E., and Nunnermacker, L. J.: Tropospheric chemistry over  
781 the lower Great-Plains of the United States. 2 Trace gas profiles and distributions, Journal of Geophysical  
782 Research-Atmospheres, 97, 20647-20670, 1992.

783 Mazzuca, G. M., Ren, X. R., Loughner, C. P., Estes, M., Crawford, J. H., Pickering, K. E., Weinheimer, A. J., and  
784 Dickerson, R. R.: Ozone production and its sensitivity to NO<sub>x</sub> and VOCs: results from the DISCOVER-AQ  
785 field experiment, Houston 2013, Atmospheric Chemistry and Physics, 16, 14463-14474, 10.5194/acp-16-  
786 14463-2016, 2016.

787 Millet, D. B., Jacob, D. J., Turquety, S., Hudman, R. C., Wu, S., Fried, A., Walega, J., Heikes, B. G., Blake, D. R.,  
788 Singh, H. B., Anderson, B. E., and Clarke, A. D.: Formaldehyde distribution over North America:  
789 Implications for satellite retrievals of formaldehyde columns and isoprene emission, Journal of Geophysical  
790 Research: Atmospheres, 111, doi:10.1029/2005JD006853, 2006.

791 Miyazaki, K., Sekiya, T., Fu, D., Bowman, K. W., Kulawik, S. S., Sudo, K., Walker, T., Kanaya, Y., Takigawa, M.,  
792 Ogochi, K., Eskes, H., Boersma, K. F., Thompson, A. M., Gaubert, B., Barre, J., and Emmons, L. K.:  
793 Balance of Emission and Dynamical Controls on Ozone During the Korea-United States Air Quality  
794 Campaign From Multiconstituent Satellite Data Assimilation, Journal of Geophysical Research:  
795 Atmospheres, 124, 387-413, 10.1029/2018jd028912, 2019.

796 MOPITT Science Team: MOPITT/Terra Level 3 Gridded Daily CO (on a latitude/longitude/pressure grid) derived  
797 from Near and Thermal Infrared Radiances, version 7, Hampton, VA, USA:NASA Atmospheric Science  
798 Data Center (ASDC), Accessed January 2018, 10.5067/TERRA/MOPITT/MOP03J\_L3.007, 2013.

799 Ni, R. J., Lin, J. T., Yan, Y. Y., and Lin, W. L.: Foreign and domestic contributions to springtime ozone over China,  
800 Atmospheric Chemistry and Physics, 18, 11447-11469, 10.5194/acp-18-11447-2018, 2018.

801 Ohara, T., Akimoto, H., Kurokawa, J., Horii, N., Yamaji, K., Yan, X., and Hayasaka, T.: An Asian emission  
802 inventory of anthropogenic emission sources for the period 1980-2020, Atmospheric Chemistry and  
803 Physics, 7, 4419-4444, 10.5194/acp-7-4419-2007, 2007.

804 Pleim, J. E., and Xiu, A.: Development and Testing of a Surface Flux and Planetary Boundary Layer Model for  
805 Application in Mesoscale Models, Journal of Applied Meteorology, 34, 16-32, 10.1175/1520-0450-34.1.16,  
806 1995.

807 Pleim, J. E.: A Combined Local and Nonlocal Closure Model for the Atmospheric Boundary Layer. Part I: Model  
808 Description and Testing, J. Appl. Meteorol. Climatol., 46, 1383-1395, 10.1175/jam2539.1, 2007.

809 Qu, Z., Henze, D. K., Capps, S. L., Wang, Y., Xu, X. G., Wang, J., and Keller, M.: Monthly top-down NO<sub>x</sub>  
810 emissions for China (2005-2012): A hybrid inversion method and trend analysis, Journal of Geophysical  
811 Research-Atmospheres, 122, 4600-4625, 10.1002/2016jd025852, 2017.

812 Ramanathan, V., and Dickinson, R. E.: Role of stratospheric ozone in the zonal and seasonal radiative energy-  
813 balance of the Earth-troposphere system, Journal of the Atmospheric Sciences, 36, 1084-1104, 1979.

814 Rappenglück, B., Dasgupta, P. K., Leuchner, M., Li, Q., and Luke, W.: Formaldehyde and its relation to CO, PAN,  
815 and SO<sub>2</sub> in the Houston-Galveston airshed, Atmos. Chem. Phys., 10, 2413-2424,  
816 10.5194/acp-10-2413-2010, 2010.

817 Ren, X., Salmon, O. E., Hansford, J. R., Ahn, D., Hall, D., Benish, S. E., Stratton, P. R., He, H., Sahu, S., Grimes,  
818 C., Heimbürger, A. M. F., Martin, C. R., Cohen, M. D., Stunder, B., Salawitch, R. J., Ehrman, S. H.,  
819 Shepson, P. B., and Dickerson, R. R.: Methane Emissions From the Baltimore-Washington Area Based on  
820 Airborne Observations: Comparison to Emissions Inventories, Journal of Geophysical Research:  
821 Atmospheres, 0, doi:10.1029/2018JD028851, 2018.

822 Ring, A. M., Canty, T. P., Anderson, D. C., Vinciguerra, T. P., He, H., Goldberg, D. L., Ehrman, S. H., Dickerson, R.  
823 R., and Salawitch, R. J.: Evaluating commercial marine emissions and their role in air quality policy using  
824 observations and the CMAQ model, Atmospheric Environment, 173, 96-107,  
825 <https://doi.org/10.1016/j.atmosenv.2017.10.037>, 2018.

826 Salmon, O. E., Shepson, P. B., Ren, X., He, H., Hall, D. L., Dickerson, R. R., Stirm, B. H., Brown, S. S., Fibiger, D.  
827 L., McDuffie, E. E., Campos, T. L., Gurney, K. R., and Thornton, J. A.: Top-Down Estimates of NO<sub>x</sub> and  
828 CO Emissions From Washington, D.C.-Baltimore During the WINTER Campaign, Journal of Geophysical  
829 Research: Atmospheres, 123, 7705-7724, doi:10.1029/2018JD028539, 2018.

830 Schroeder, J. R., Crawford, J. H., Fried, A., Walega, J., Weinheimer, A., Wisthaler, A., Muller, M., Mikoviny, T.,  
831 Chen, G., Shook, M., Blake, D. R., and Tonnesen, G. S.: New insights into the column CH<sub>2</sub>O/NO<sub>2</sub> ratio as  
832 an indicator of near-surface ozone sensitivity, Journal of Geophysical Research-Atmospheres, 122, 8885-  
833 8907, 10.1002/2017jd026781, 2017.

834 Seinfeld, J. H., and Pandis, S. N.: Atmospheric Chemistry and Physics: From Air Pollution to Climate Change, 2nd  
835 ed., John Wiley & Sons, Inc., 2006.

836 Shan, Y., Guan, D., Zheng, H., Ou, J., Li, Y., Meng, J., Mi, Z., Liu, Z., and Zhang, Q.: China CO<sub>2</sub> emission accounts  
837 1997–2015, Scientific Data, 5, 170201, 10.1038/sdata.2017.201,  
838 <https://www.nature.com/articles/sdata2017201#supplementary-information>, 2018.

839 Sillman, S.: The relation between ozone, NO<sub>x</sub> and hydrocarbons in urban and polluted rural environments,  
840 Atmospheric Environment, 33, 1821-1845, 10.1016/s1352-2310(98)00345-8, 1999.

841 Skamarock, W. C., Klemp, J. B., Dudhia, J., Gill, D. O., Barker, D. M., Duda, M. G., Huang, X.-Y., Wang, W., and  
842 Powers, J. G.: A Description of the Advanced Research WRF Version 3, NCAR Technical Note,  
843 NCAR/TN-475+STR, 113 pp, 2008.

844 Stavrakou, T., Muller, J. F., Bauwens, M., De Smedt, I., Lerot, C., Van Roozendaal, M., Coheur, P. F., Clerbaux, C.,  
845 Boersma, K. F., van der A, R., and Song, Y.: Substantial Underestimation of Post-Harvest Burning  
846 Emissions in the North China Plain Revealed by Multi-Species Space Observations, Scientific Reports, 6,  
847 32307, 10.1038/srep32307, 2016.

848 Stehr, J. W., Dickerson, R. R., Hallock-Waters, K. A., Doddridge, B. G., and Kirk, D.: Observations of NO<sub>y</sub>, CO,  
849 and SO<sub>2</sub> and the origin of reactive nitrogen in the eastern United States, Journal of Geophysical Research-  
850 Atmospheres, 105, 3553-3563, 2000.

851 Stevenson, D. S., Dentener, F. J., Schultz, M. G., Ellingsen, K., van Noije, T. P. C., Wild, O., Zeng, G., Amann, M.,  
852 Atherton, C. S., Bell, N., Bergmann, D. J., Bey, I., Butler, T., Cofala, J., Collins, W. J., Derwent, R. G.,  
853 Doherty, R. M., Drevet, J., Eskes, H. J., Fiore, A. M., Gauss, M., Hauglustaine, D. A., Horowitz, L. W.,  
854 Isaksen, I. S. A., Krol, M. C., Lamarque, J. F., Lawrence, M. G., Montanaro, V., Muller, J. F., Pitari, G.,  
855 Prather, M. J., Pyle, J. A., Rast, S., Rodriguez, J. M., Sanderson, M. G., Savage, N. H., Shindell, D. T.,  
856 Strahan, S. E., Sudo, K., and Szopa, S.: Multimodel ensemble simulations of present-day and near-future  
857 tropospheric ozone, Journal of Geophysical Research-Atmospheres, 111, D08301, 10.1029/2005jd006338,  
858 2006.

859 Streets, D. G., Bond, T. C., Carmichael, G. R., Fernandes, S. D., Fu, Q., He, D., Klimont, Z., Nelson, S. M., Tsai, N.  
860 Y., Wang, M. Q., Woo, J. H., and Yarber, K. F.: An inventory of gaseous and primary aerosol emissions in  
861 Asia in the year 2000, Journal of Geophysical Research-Atmospheres, 108, 8809, 10.1029/2002jd003093,  
862 2003.

863 Sun, Y. L., Zhuang, G. S., Tang, A. H., Wang, Y., and An, Z. S.: Chemical characteristics of PM<sub>2.5</sub> and PM<sub>10</sub> in  
864 haze-fog episodes in Beijing, Environmental Science & Technology, 40, 3148-3155, 10.1021/es051533g,  
865 2006.

866 Taubman, B. F., Hains, J. C., Thompson, A. M., Marufu, L. T., Doddridge, B. G., Stehr, J. W., Piety, C. A., and  
867 Dickerson, R. R.: Aircraft vertical profiles of trace gas and aerosol pollution over the mid-Atlantic United  
868 States: Statistics and meteorological cluster analysis, Journal of Geophysical Research-Atmospheres, 111,  
869 D10s07 10.1029/2005jd006196, 2006.

870 Thompson, A. M.: The oxidizing capacity of the Earth's Atmosphere - probable past and future changes, Science,  
871 256, 1157-1165, 10.1126/science.256.5060.1157, 1992.

872 Tie, X. X., Wu, D., and Brasseur, G.: Lung cancer mortality and exposure to atmospheric aerosol particles in  
873 Guangzhou, China, Atmospheric Environment, 43, 2375-2377, 10.1016/j.atmosenv.2009.01.036, 2009.

874 UNC: SMOKE v4.5 User's Manual, The Institute for the Environment, The University of North Carolina at Chapel  
875 Hill, 2017.

876 Verstraeten, W. W., Neu, J. L., Williams, J. E., Bowman, K. W., Worden, J. R., and Boersma, K. F.: Rapid increases  
877 in tropospheric ozone production and export from China, Nature Geoscience, 8, 690-+, 10.1038/ngeo2493,  
878 2015.

879 Wang, F., Li, Z., Ren, X., Jiang, Q., He, H., Dickerson, R. R., Dong, X., and Lv, F.: Vertical distributions of aerosol  
880 optical properties during the spring 2016 ARIAs airborne campaign in the North China Plain, Atmos.  
881 Chem. Phys., 18, 8995-9010, 10.5194/acp-18-8995-2018, 2018a.

882 Wang, R., Xu, X. B., Jia, S. H., Ma, R. S., Ran, L., Deng, Z. Z., Lin, W. L., Wang, Y., and Ma, Z. Q.: Lower  
883 tropospheric distributions of O<sub>3</sub> and aerosol over Raoyang, a rural site in the North China Plain,  
884 Atmospheric Chemistry and Physics, 17, 3891-3903, 10.5194/acp-17-3891-2017, 2017a.

885 Wang, S. W., Zhang, Q., Streets, D. G., He, K. B., Martin, R. V., Lamsal, L. N., Chen, D., Lei, Y., and Lu, Z.:  
886 Growth in NO<sub>x</sub> emissions from power plants in China: bottom-up estimates and satellite observations,  
887 Atmospheric Chemistry and Physics, 12, 4429-4447, 10.5194/acp-12-4429-2012, 2012.

888 Wang, S. X., and Hao, J. M.: Air quality management in China: Issues, challenges, and options, J. Environ. Sci., 24,  
889 2-13, 10.1016/s1001-0742(11)60724-9, 2012.

890 Wang, S. X., Xing, J., Zhao, B., Jang, C., and Hao, J. M.: Effectiveness of national air pollution control policies on  
891 the air quality in metropolitan areas of China, *J. Environ. Sci.*, 26, 13-22, 10.1016/s1001-0742(13)60381-2,  
892 2014a.

893 Wang, T., Xue, L. K., Brimblecombe, P., Lam, Y. F., Li, L., and Zhang, L.: Ozone pollution in China: A review of  
894 concentrations, meteorological influences, chemical precursors, and effects, *Science of the Total*  
895 *Environment*, 575, 1582-1596, 10.1016/j.scitotenv.2016.10.081, 2017b.

896 Wang, Y., Zhuang, G. S., Tang, A. H., Yuan, H., Sun, Y. L., Chen, S. A., and Zheng, A. H.: The ion chemistry and the  
897 source of PM<sub>2.5</sub> aerosol in Beijing, *Atmospheric Environment*, 39, 3771-3784,  
898 10.1016/j.atmosenv.2005.03.013, 2005.

899 Wang, Y., Li, Z., Zhang, Y., Du, W., Zhang, F., Tan, H., Xu, H., Fan, T., Jin, X., Fan, X., Dong, Z., Wang, Q., and  
900 Sun, Y.: Characterization of aerosol hygroscopicity, mixing state, and CCN activity at a suburban site in the  
901 central North China Plain, *Atmos. Chem. Phys.*, 18, 11739-11752, 10.5194/acp-18-11739-2018, 2018b.

902 Wang, Y. S., Yao, L., Wang, L. L., Liu, Z. R., Ji, D. S., Tang, G. Q., Zhang, J. K., Sun, Y., Hu, B., and Xin, J. Y.:  
903 Mechanism for the formation of the January 2013 heavy haze pollution episode over central and eastern  
904 China, *Sci. China-Earth Sci.*, 57, 14-25, 10.1007/s11430-013-4773-4, 2014b.

905 Wei, W., Wang, S. X., Hao, J. M., and Cheng, S. Y.: Projection of anthropogenic volatile organic compounds (VOCs)  
906 emissions in China for the period 2010-2020, *Atmospheric Environment*, 45, 6863-6871,  
907 10.1016/j.atmosenv.2011.01.013, 2011.

908 WHO: Health aspects of air pollution with particulate matter, ozone and nitrogen dioxide, *World Health*  
909 *Organisation, Bonn.*, 2003.

910 Worden, H. M., Deeter, M. N., Edwards, D. P., Gille, J. C., Drummond, J. R., and Nedelec, P.: Observations of near-  
911 surface carbon monoxide from space using MOPITT multispectral retrievals, *Journal of Geophysical*  
912 *Research-Atmospheres*, 115, D18314, 10.1029/2010jd014242, 2010.

913 Xing, J., Wang, S. X., Jang, C., Zhu, Y., and Hao, J. M.: Nonlinear response of ozone to precursor emission changes  
914 in China: a modeling study using response surface methodology, *Atmospheric Chemistry and Physics*, 11,  
915 5027-5044, 10.5194/acp-11-5027-2011, 2011.

916 Xing, J., Ding, D., Wang, S. X., Zhao, B., Jang, C., Wu, W. J., Zhang, F. F., Zhu, Y., and Hao, J. M.: Quantification  
917 of the enhanced effectiveness of NO<sub>x</sub> control from simultaneous reductions of VOC and NH<sub>3</sub> for reducing  
918 air pollution in the Beijing-Tianjin-Hebei region, China, *Atmospheric Chemistry and Physics*, 18, 7799-  
919 7814, 10.5194/acp-18-7799-2018, 2018.

920 Xiu, A., and Pleim, J. E.: Development of a Land Surface Model. Part I: Application in a Mesoscale Meteorological  
921 Model, *Journal of Applied Meteorology*, 40, 192-209, 10.1175/1520-  
922 0450(2001)040<0192:doalsm>2.0.co;2, 2001.

923 Xue, L. K., Wang, T., Gao, J., Ding, A. J., Zhou, X. H., Blake, D. R., Wang, X. F., Saunders, S. M., Fan, S. J., Zuo,  
924 H. C., Zhang, Q. Z., and Wang, W. X.: Ground-level ozone in four Chinese cities: precursors, regional  
925 transport and heterogeneous processes, *Atmospheric Chemistry and Physics*, 14, 13175-13188,  
926 10.5194/acp-14-13175-2014, 2014.

927 Yang, F., Tan, J., Zhao, Q., Du, Z., He, K., Ma, Y., Duan, F., and Chen, G.: Characteristics of PM<sub>2.5</sub> speciation in  
928 representative megacities and across China, *Atmospheric Chemistry and Physics*, 11, 5207-5219,  
929 10.5194/acp-11-5207-2011, 2011.

930 Yarwood, G. S., Rao, S. T., Yocke, M., and Whitten, G. Z.: Updates to the Carbon Bond Chemical Mechanism:  
931 CB05, ENVIRON International Corp, 2005.

932 Yarwood, G. S., Whitten, G. Z., Jung, J., Heo, G., and Allen, D.: Development, Evaluation and Testing of Version 6  
933 of the Carbon Bond Chemical Mechanism (CB6),  
934 [https://www.tceq.texas.gov/assets/public/implementation/air/am/contracts/reports/pm/5820784005FY1026-  
935 20100922-environ-cb6.pdf](https://www.tceq.texas.gov/assets/public/implementation/air/am/contracts/reports/pm/5820784005FY1026-20100922-environ-cb6.pdf), 2010.

936 Ye, B. M., Ji, X. L., Yang, H. Z., Yao, X. H., Chan, C. K., Cadle, S. H., Chan, T., and Mulawa, P. A.: Concentration  
937 and chemical composition of PM<sub>2.5</sub> in Shanghai for a 1-year period, *Atmospheric Environment*, 37, 499-  
938 510, Pii s1352-2310(02)00918-4, 10.1016/s1352-2310(02)00918-4, 2003.

939 Young, P. J., Archibald, A. T., Bowman, K. W., Lamarque, J. F., Naik, V., Stevenson, D. S., Tilmes, S., Voulgarakis,  
940 A., Wild, O., Bergmann, D., Cameron-Smith, P., Cionni, I., Collins, W. J., Dalsoren, S. B., Doherty, R. M.,  
941 Eyring, V., Faluvegi, G., Horowitz, L. W., Josse, B., Lee, Y. H., MacKenzie, I. A., Nagashima, T., Plummer,  
942 D. A., Righi, M., Rumbold, S. T., Skeie, R. B., Shindell, D. T., Strode, S. A., Sudo, K., Szopa, S., and Zeng,  
943 G.: Pre-industrial to end 21st century projections of tropospheric ozone from the Atmospheric Chemistry  
944 and Climate Model Intercomparison Project (ACCMIP), *Atmospheric Chemistry and Physics*, 13, 2063-  
945 2090, 10.5194/acp-13-2063-2013, 2013.

946 Zhang, J. N., Xiao, J. F., Chen, X. F., Liang, X. M., Fan, L. Y., and Ye, D. Q.: Allowance and allocation of industrial  
947 volatile organic compounds emission in China for year 2020 and 2030, *J. Environ. Sci.*, 69, 155-165,  
948 10.1016/j.jes.2017.10.003, 2018.

949 Zhang, R., Jing, J., Tao, J., Hsu, S. C., Wang, G., Cao, J., Lee, C. S. L., Zhu, L., Chen, Z., Zhao, Y., and Shen, Z.:  
950 Chemical characterization and source apportionment of PM<sub>2.5</sub> in Beijing: seasonal perspective,  
951 *Atmospheric Chemistry and Physics*, 13, 7053-7074, 10.5194/acp-13-7053-2013, 2013.

952 Zhang, W., Zhu, T., Yang, W., Bai, Z., Sun, Y. L., Xu, Y., Yin, B., and Zhao, X.: Airborne measurements of gas and  
953 particle pollutants during CAREBeijing-2008, *Atmospheric Chemistry and Physics*, 14, 301-316,  
954 10.5194/acp-14-301-2014, 2014.

955 Zhang, X. P., and Cheng, X. M.: Energy consumption, carbon emissions, and economic growth in China, *Ecological  
956 Economics*, 68, 2706-2712, 10.1016/j.ecolecon.2009.05.011, 2009.

957 Zhang, X. Y., Wang, Y. Q., Niu, T., Zhang, X. C., Gong, S. L., Zhang, Y. M., and Sun, J. Y.: Atmospheric aerosol  
958 compositions in China: spatial/temporal variability, chemical signature, regional haze distribution and  
959 comparisons with global aerosols, *Atmospheric Chemistry and Physics*, 12, 779-799, 10.5194/acp-12-779-  
960 2012, 2012.

961 Zhao, B., Wang, S. X., Liu, H., Xu, J. Y., Fu, K., Klimont, Z., Hao, J. M., He, K. B., Cofala, J., and Amann, M.: NO<sub>x</sub>  
962 emissions in China: historical trends and future perspectives, *Atmospheric Chemistry and Physics*, 13,  
963 9869-9897, 10.5194/acp-13-9869-2013, 2013a.

964 Zhao, P. S., Dong, F., He, D., Zhao, X. J., Zhang, X. L., Zhang, W. Z., Yao, Q., and Liu, H. Y.: Characteristics of  
965 concentrations and chemical compositions for PM<sub>2.5</sub> in the region of Beijing, Tianjin, and Hebei, China,  
966 *Atmospheric Chemistry and Physics*, 13, 4631-4644, 10.5194/acp-13-4631-2013, 2013b.

967 Zhao, Y., Zhang, J., and Nielsen, C. P.: The effects of recent control policies on trends in emissions of anthropogenic  
968 atmospheric pollutants and CO<sub>2</sub> in China, *Atmospheric Chemistry and Physics*, 13, 487-508, 10.5194/acp-  
969 13-487-2013, 2013c.

970 Zhao, Y., Mao, P., Zhou, Y., Yang, Y., Zhang, J., Wang, S., Dong, Y., Xie, F., Yu, Y., and Li, W.: Improved provincial  
971 emission inventory and speciation profiles of anthropogenic non-methane volatile organic compounds: a  
972 case study for Jiangsu, China, *Atmos. Chem. Phys.*, 17, 7733-7756, 10.5194/acp-17-7733-2017, 2017.

973 Zheng, B., Chevallier, F., Ciais, P., Yin, Y., Deeter, M. N., Worden, H. M., Wang, Y. L., Zhang, Q., and He, K. B.:  
974 Rapid decline in carbon monoxide emissions and export from East Asia between years 2005 and 2016,  
975 *Environ. Res. Lett.*, 13, 044007, 10.1088/1748-9326/aab2b3, 2018.

976 Zhu, Y., Zhang, J., Wang, J., Chen, W., Han, Y., Ye, C., Li, Y., Liu, J., Zeng, L., Wu, Y., Wang, X., Wang, W., Chen,  
977 J., and Zhu, T.: Distribution and sources of air pollutants in the North China Plain based on on-road mobile  
978 measurements, *Atmos. Chem. Phys.*, 16, 12551-12565, 10.5194/acp-16-12551-2016, 2016.

979  
980

981 **Tables and Figures**

982

983 **Table 1.** List of CMAQ simulations with adjusted emissions based on satellite observations.  
 984 Anthropogenic CO, NO<sub>x</sub>, and VOCs emissions were adjusted using MOPITT CO, OMI NO<sub>2</sub>, and  
 985 OMI HCHO observations.

986

Run NO.	Experiment Name	Bio. VOCs	Anthro. CO	Anthro. NO <sub>x</sub>	Anthro. VOCs
1	CMAQ_baseline	BEIS	EDGAR	EDGAR	EDGAR
2	CMAQ_noBEIS	N/A	EDGAR	EDGAR	EDGAR
3	CMAQ_CO	BEIS	Adjusted	EDGAR	EDGAR
4	CMAQ_NO <sub>x</sub>	BEIS	EDGAR	Adjusted	EDGAR
5	CMAQ_VOCs	BEIS	EDGAR	EDGAR	Adjusted
6	CMAQ_All	BEIS	Adjusted	Adjusted	Adjusted

987

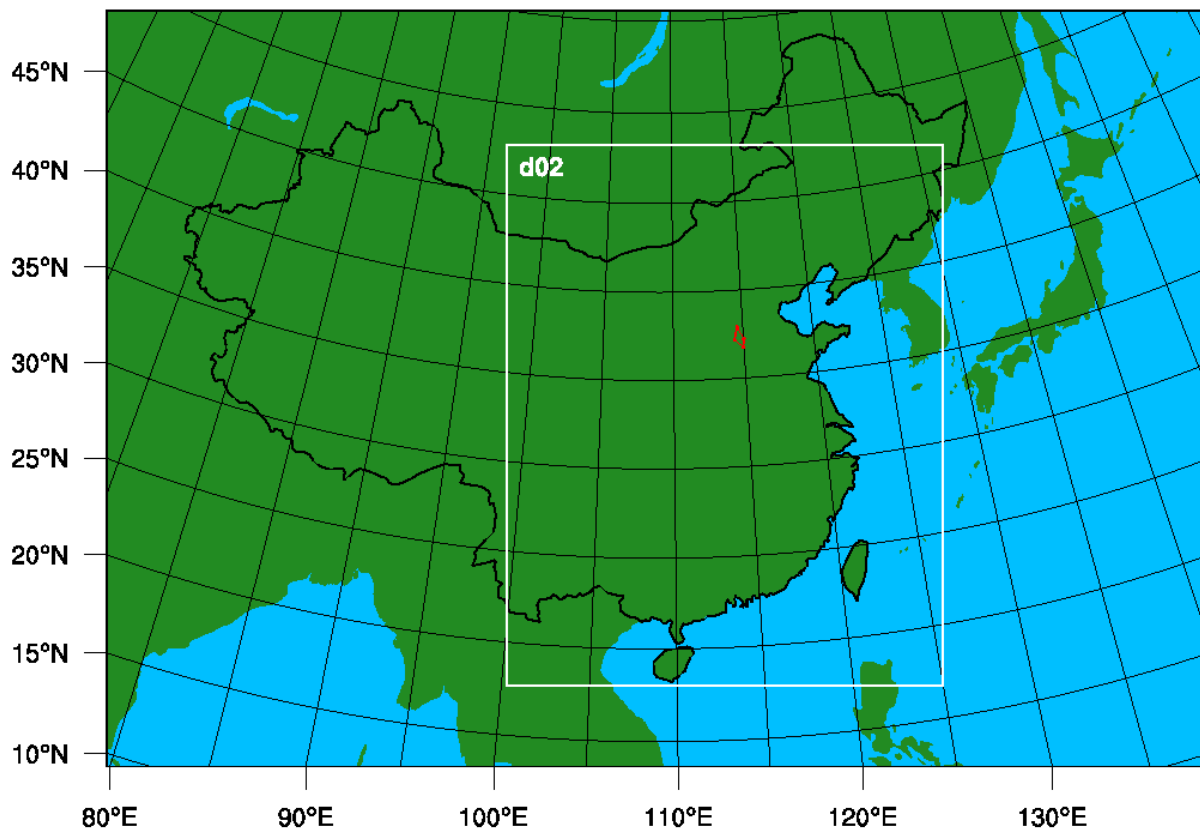
988  
989  
990

**Table 2.** Statistics of CMAQ performance of six sensitivity experiments compared with ARIAs aircraft measurements over the NCP.

No	Name	Mean Diff	Slope	Stdev	Corr. R	NMB	NME	RMSE	Mean Ratio
		ppbv	Unitless	ppbv	Unitless	%	%	ppbv	Unitless
O <sub>3</sub>									
1	CMAQ_Baseline	-21.35	0.56	13.25	0.37	-25.14	25.86	25.10	0.75
2	CMAQ_noBEIS	-23.74	0.49	12.85	0.41	-27.94	28.34	26.97	0.72
3	CMAQ_NOx	-19.83	0.59	13.63	0.34	-23.34	24.18	24.03	0.77
4	CMAQ_VOCs	-19.26	0.66	13.66	0.36	-22.67	23.81	23.58	0.77
5	CMAQ_CO	-20.35	0.61	13.52	0.36	-23.96	24.83	24.40	0.76
6	CMAQ_All	-15.18	0.81	14.83	0.33	-17.87	20.33	21.18	0.82
CO									
1	CMAQ_Baseline	-183.56	0.21	165.92	0.23	-60.26	60.26	246.98	0.40
2	CMAQ_noBEIS	-186.34	0.21	165.52	0.25	-61.17	61.17	248.79	0.39
3	CMAQ_NOx	-184.25	0.21	165.76	0.24	-60.48	60.50	247.39	0.40
4	CMAQ_VOCs	-181.89	0.22	166.32	0.22	-59.71	59.78	246.01	0.40
5	CMAQ_CO	-148.55	0.36	167.90	0.22	-48.76	50.32	223.67	0.51
6	CMAQ_All	-104.45	0.52	175.48	0.21	-34.29	45.03	203.60	0.66
NO <sub>2</sub>									
1	CMAQ_Baseline	-1.72	0.31	3.09	0.58	-59.91	64.59	3.52	0.40
2	CMAQ_noBEIS	-1.73	0.31	3.09	0.58	-60.47	64.90	3.52	0.40
3	CMAQ_NOx	-1.45	0.38	2.99	0.60	-50.61	61.26	3.31	0.49
4	CMAQ_VOCs	-1.76	0.31	3.10	0.58	-61.60	65.66	3.55	0.38
5	CMAQ_CO	-1.70	0.31	3.09	0.58	-59.28	64.20	3.51	0.41
6	CMAQ_All	-1.47	0.38	3.01	0.59	-51.23	61.62	3.33	0.49
NO									
1	CMAQ_Baseline	-0.25	0.99	0.47	0.68	-32.23	45.4	0.53	0.68
2	CMAQ_noBEIS	-0.24	1.02	0.48	0.68	-31.09	45.66	0.54	0.69
3	CMAQ_NOx	-0.08	1.31	0.59	0.67	-9.75	50.01	0.59	0.90
4	CMAQ_VOCs	-0.30	0.89	0.45	0.68	-38.63	46.58	0.54	0.61
5	CMAQ_CO	-0.26	0.96	0.47	0.68	-33.08	45.26	0.53	0.67
6	CMAQ_All	-0.16	1.13	0.52	0.67	-20.31	45.46	0.54	0.80
NO <sub>y</sub>									
1	CMAQ_Baseline	-15.26	0.30	10.15	0.39	-77.58	77.58	18.27	0.22
2	CMAQ_noBEIS	-15.50	0.29	10.15	0.40	-78.81	78.81	18.47	0.21
3	CMAQ_NOx	-14.24	0.37	10.20	0.37	-72.39	72.39	17.46	0.28
4	CMAQ_VOCs	-15.23	0.30	10.16	0.39	-77.42	77.42	18.25	0.23
5	CMAQ_CO	-15.26	0.30	10.15	0.39	-77.56	77.56	18.27	0.22
6	CMAQ_All	-14.21	0.37	10.20	0.37	-72.26	72.26	17.44	0.28

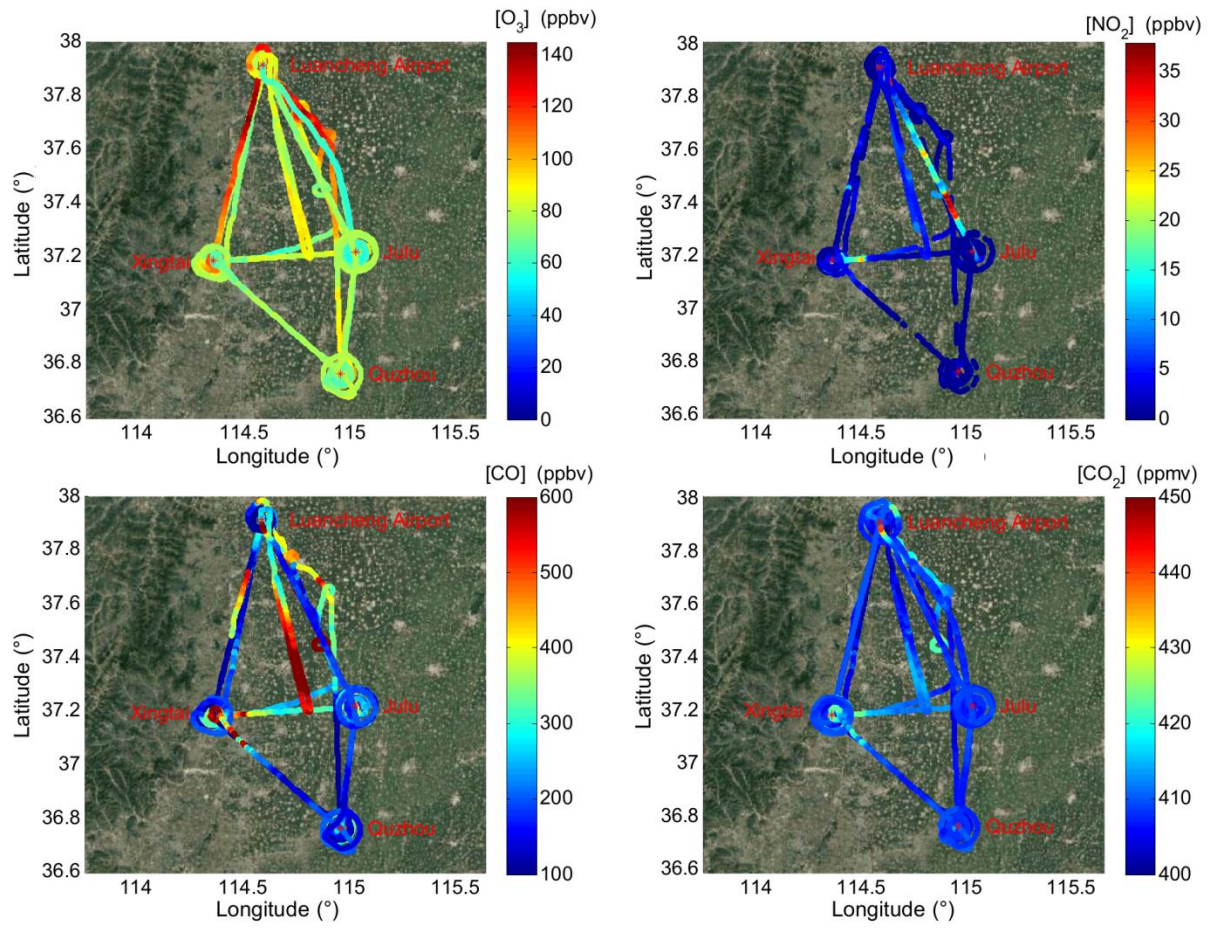
991

992 **Figure 1.** CMAQ domains for the ARIAs campaign (the proximate aircraft campaign area is  
993 demonstrated by a red polygon). The coarse domain (d01, 36 km resolution) covering East Asia  
994 and the nested domain (d02, 12 km resolution) focusing on eastern China.



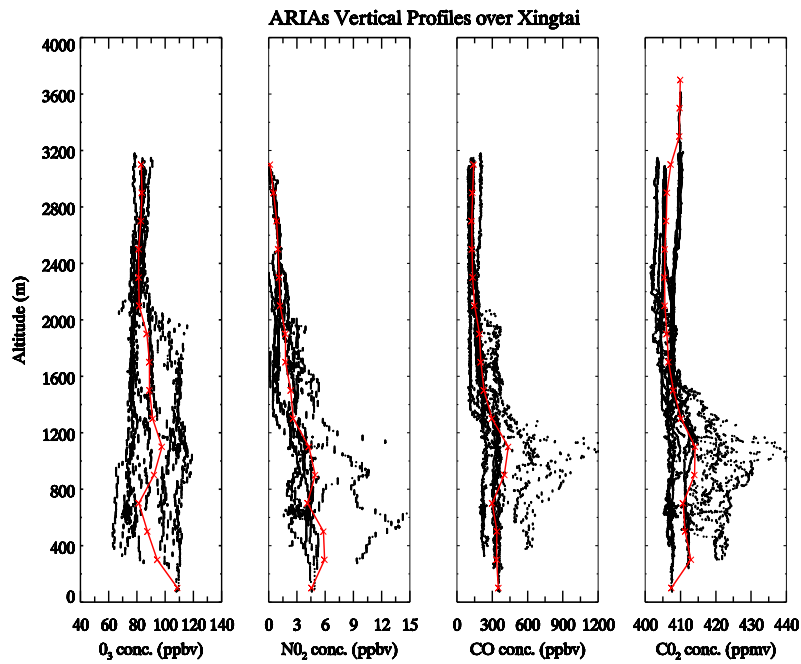
995  
996  
997  
998

999 **Figure 2.** Summary of air pollutant concentrations in the NCP observed by Y12 aircraft. a) O<sub>3</sub>, b)  
1000 NO<sub>2</sub>, c) CO, and d) CO<sub>2</sub>.  
1001

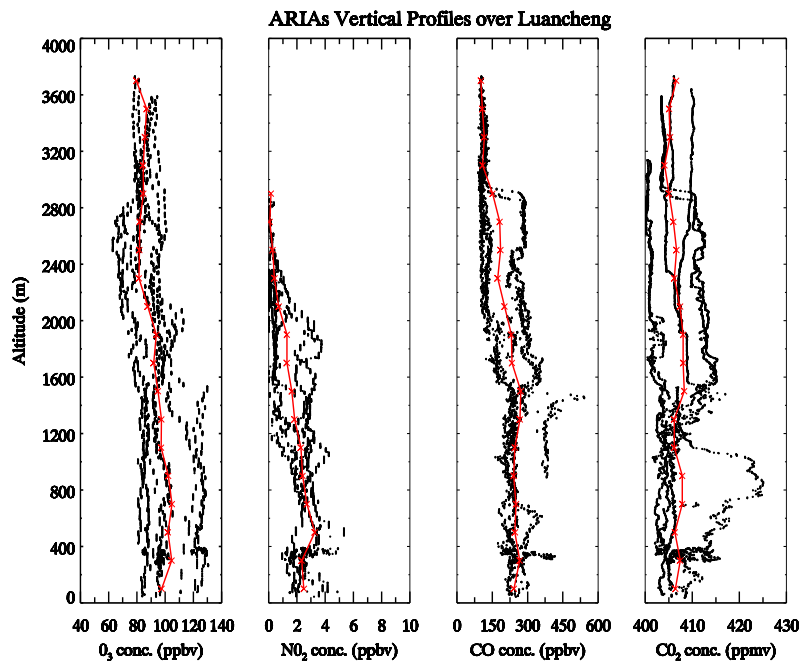


1002  
1003

1004 **Figure 3.** Vertical profiles of air pollutants over four locations in the NCP. a) Xingtai (XT), b)  
 1005 Luancheng (LC), c) Julu (JL), and d) Quzhou (QZ). Red lines show the mean profiles.  
 1006 a)

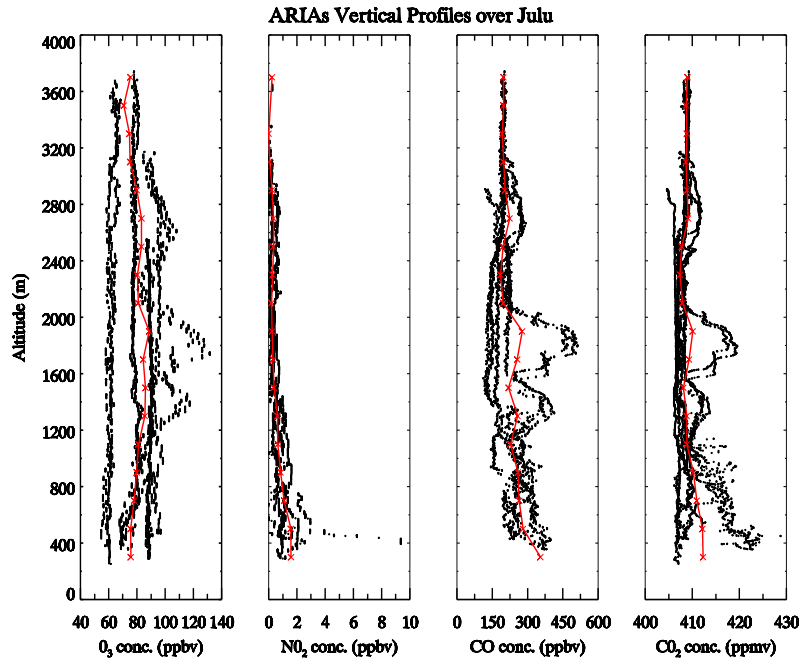


1007  
 1008 b)

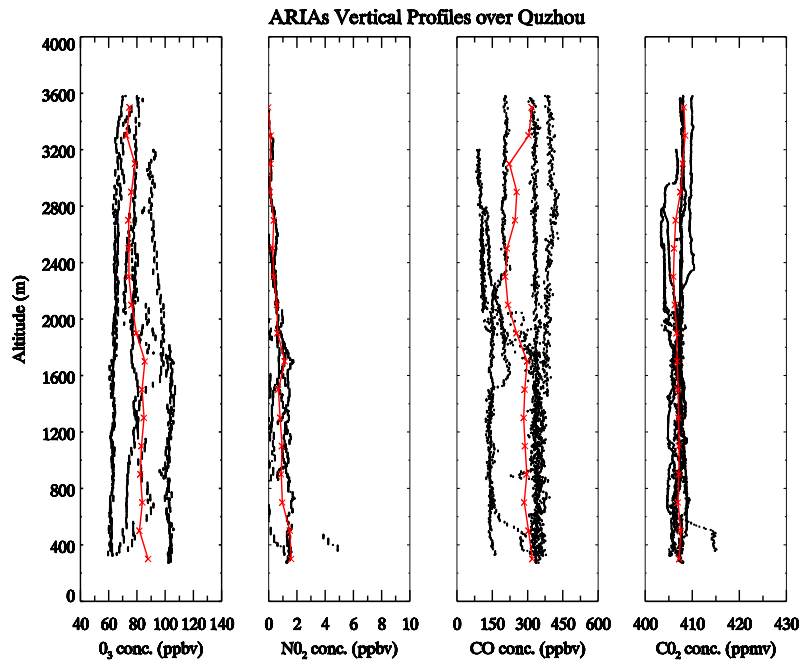


1009

1010 c)

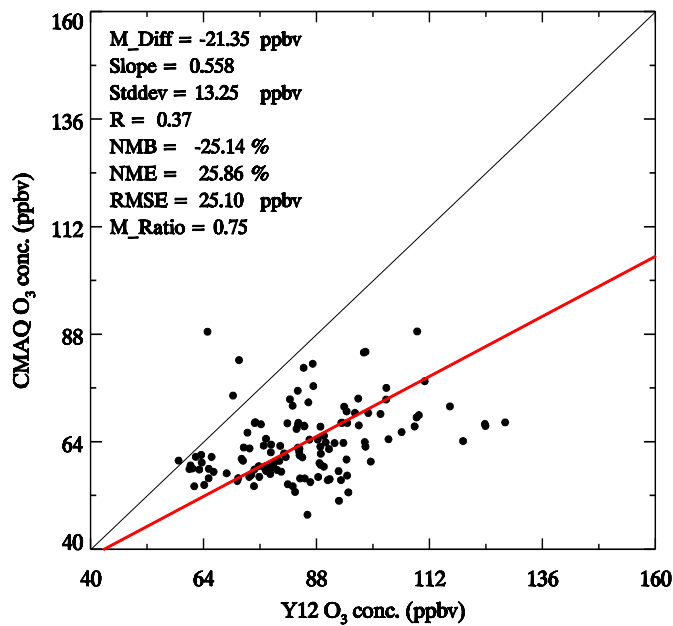


1011  
1012 d)



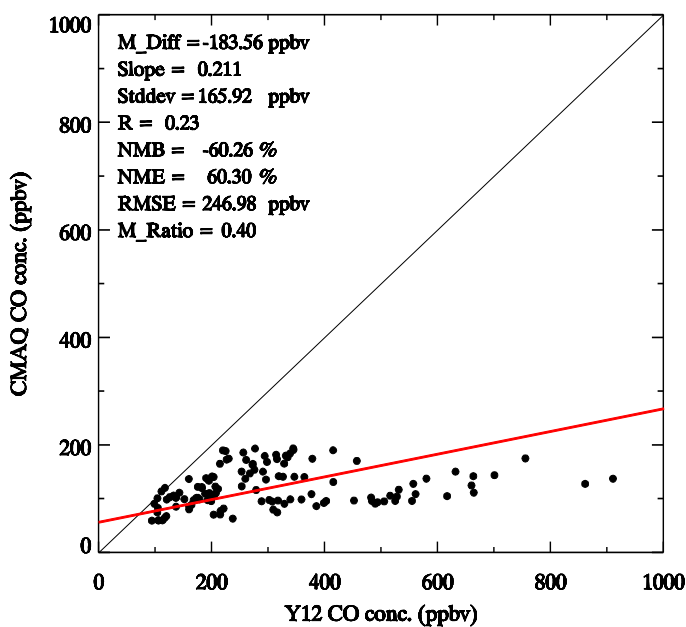
1013

1014 **Figure 4.** Comparison of 10-min averaged aircraft data and CMAQ simulations from 11 ARIAs  
 1015 research flights. a) O<sub>3</sub>, b) CO, c) NO, and d) NO<sub>2</sub>. Black line shows the 1:1 ratio; red line stands  
 1016 for the linear regression fitting line. M\_Diff: mean difference; R: correlation; NMB: normalized  
 1017 mean bias; NME: normalized mean error; RMSE: root-mean square error; M\_Ratio: mean ratio.  
 1018 a)



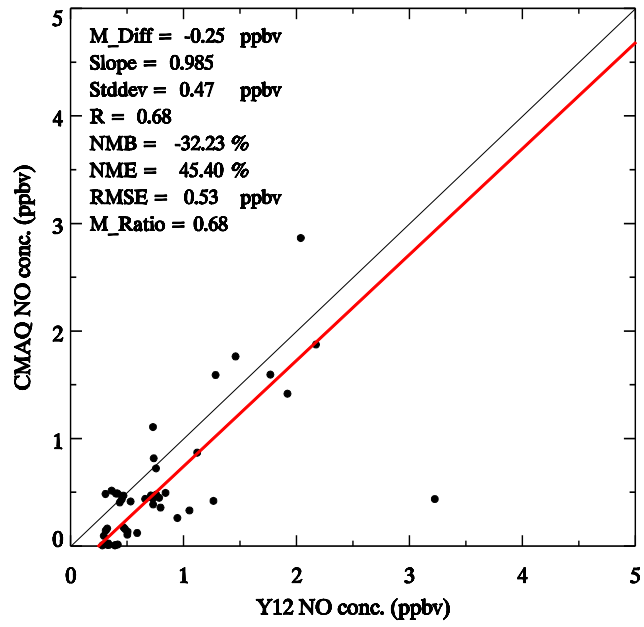
1019

1020 b)



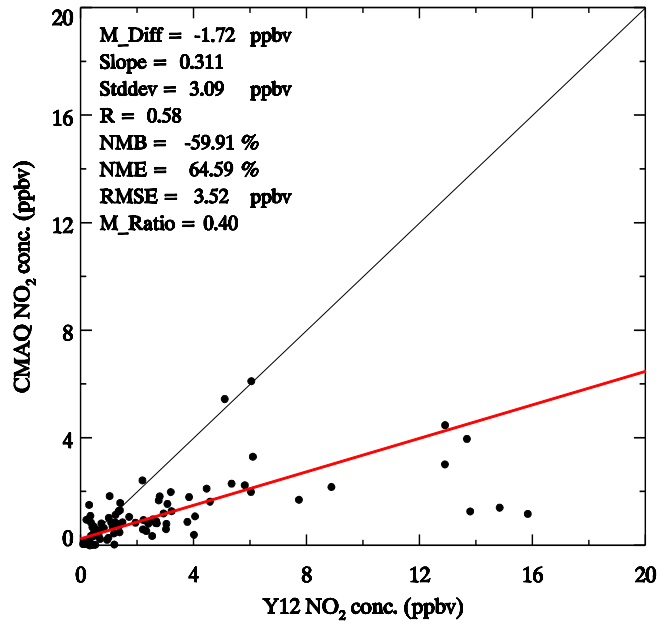
1021

1022 c)



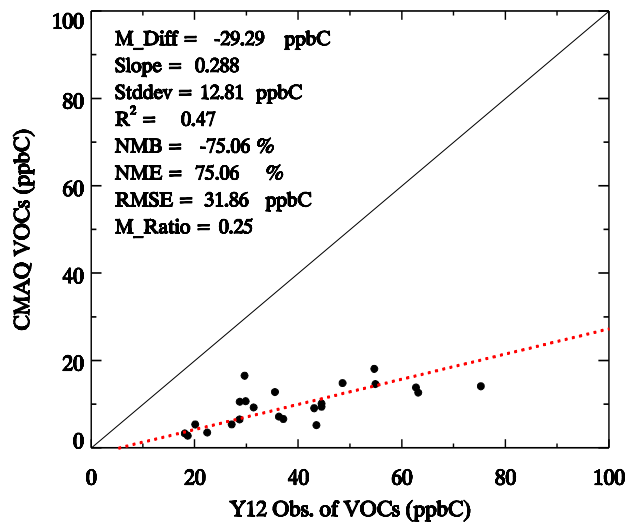
1023

1024 d)



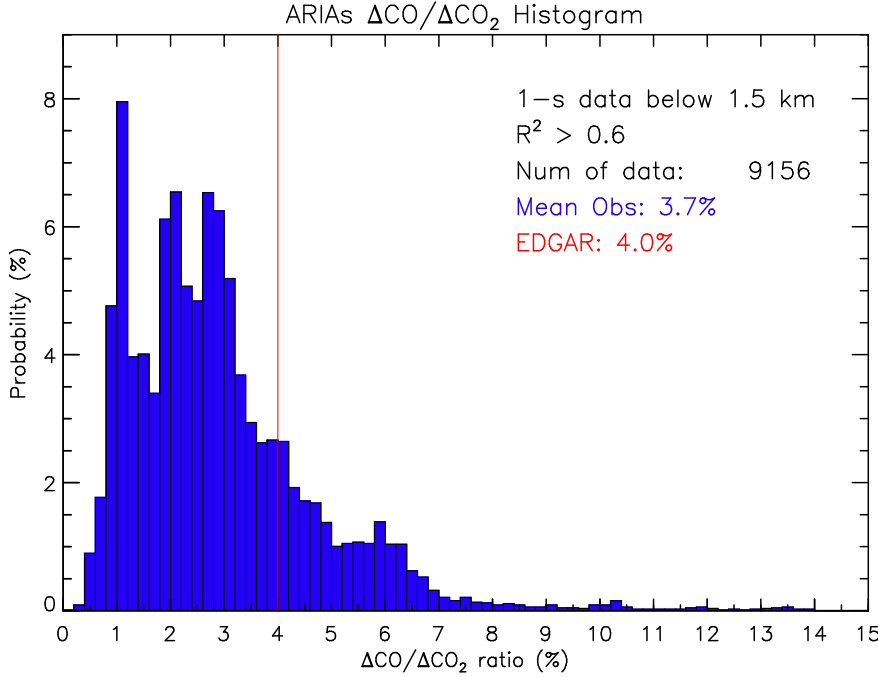
1025

1026 **Figure 5.** Comparison of total VOCs concentrations from WAS samples and CMAQ simulations.  
1027 Values are in unit of parts per billion Carbon (ppbC). Black line shows the 1:1 ratio; red line  
1028 stands for the linear regression fitting line. M\_Diff: mean difference; R: correlation; NMB:  
1029 normalized mean bias; NME: normalized mean error; RMSE: root-mean square error; M\_Ratio:  
1030 mean ratio.

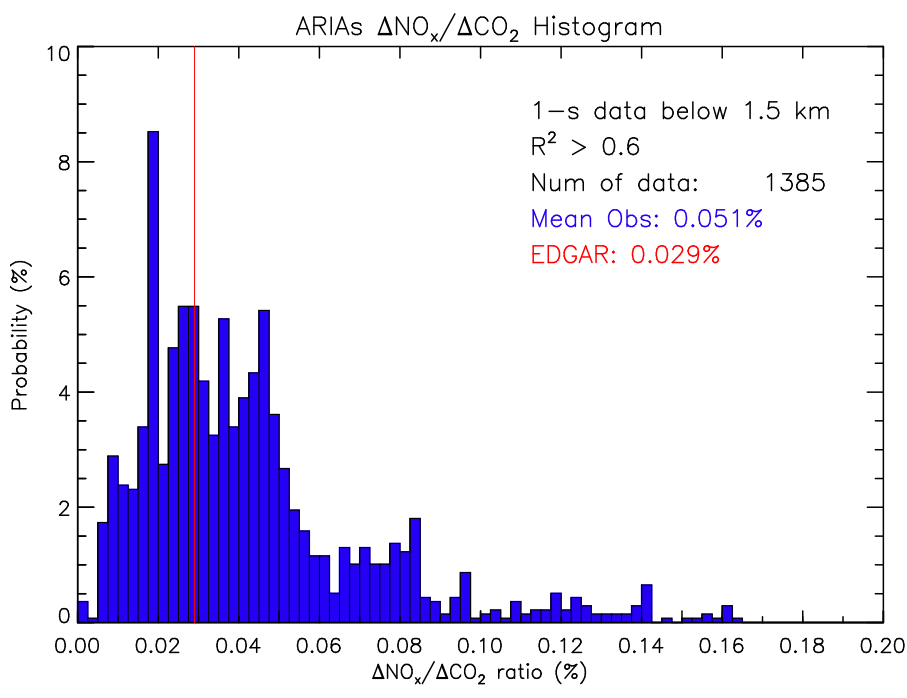


1031

1032 **Figure 6.** Comparison of emission enhancements (EEs) from the ARIAs campaign and emission  
 1033 factors (EFs) from the EDGAR emission inventory. a)  $\Delta\text{CO}/\Delta\text{CO}_2$ , b)  $\Delta\text{NO}_x/\Delta\text{CO}_2$ , c)  
 1034  $\Delta\text{NO}_x/\Delta\text{CO}$ . Blue histogram shows the distribution of EEs observed by the Y12 aircraft; red line  
 1035 shows the ratio calculated through averaging EFs from 4 sectors of the EDGAR anthropogenic  
 1036 emissions inventory.  
 1037 a)

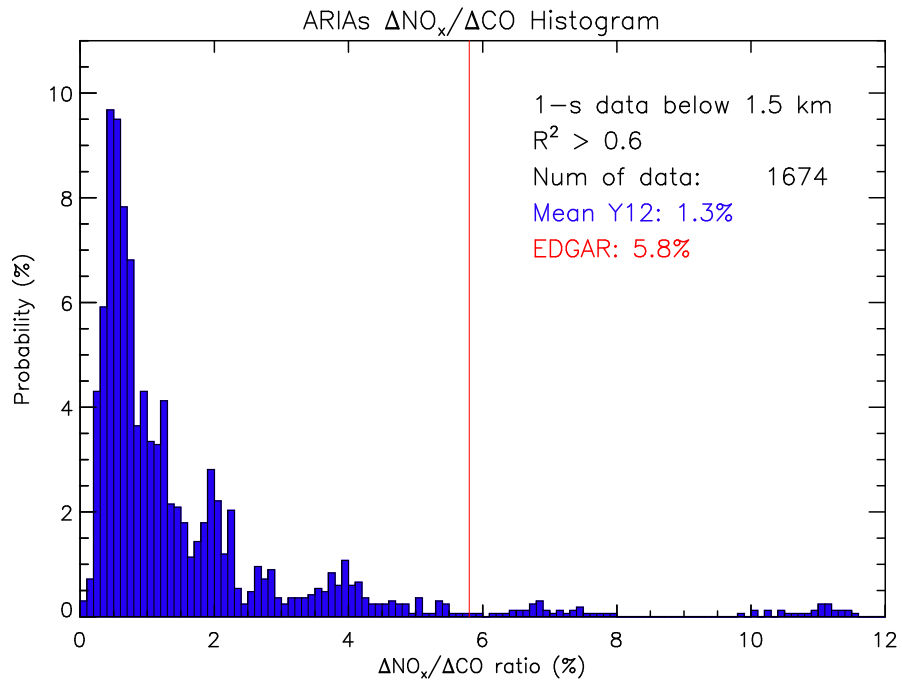


1038  
 1039 b)



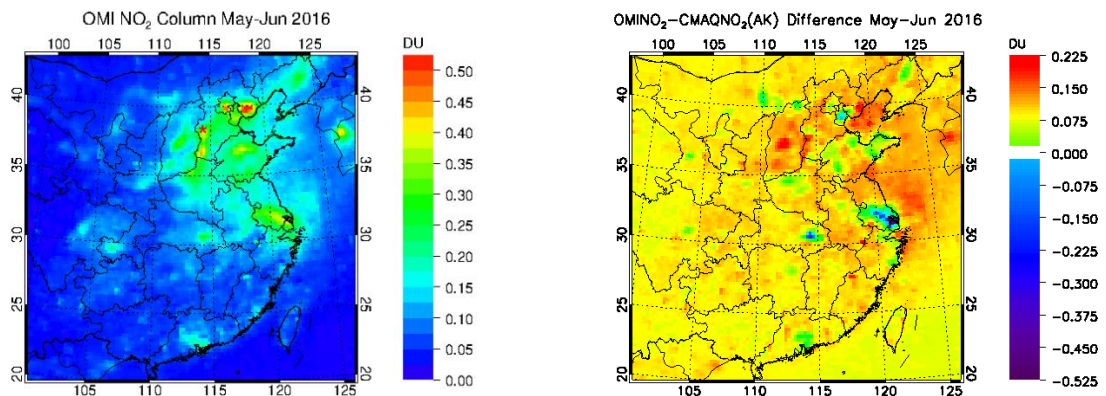
1040  
 1041

1042 c)

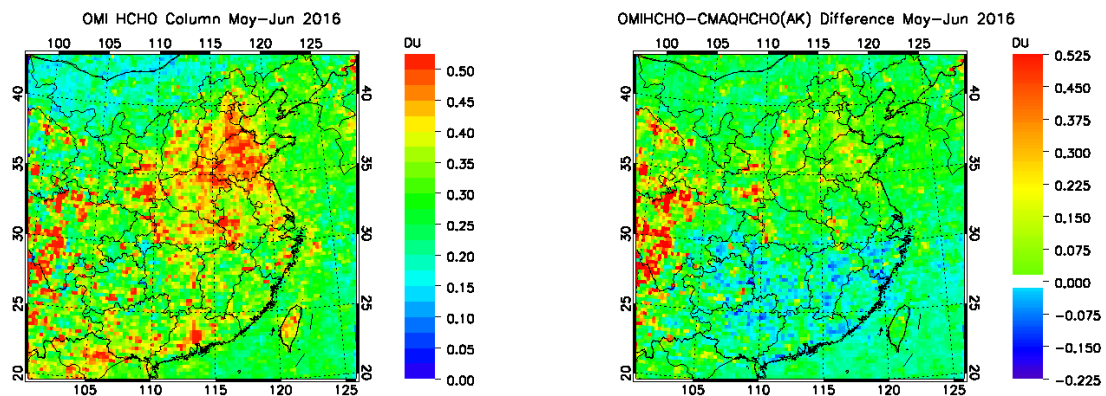


1043

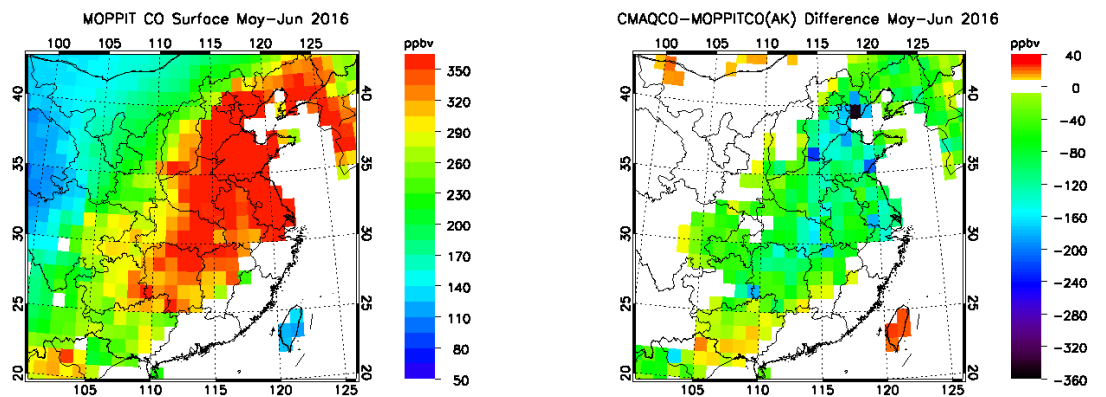
1044 **Figure 7.** Comparison of air pollutants from satellite observations and CMAQ simulations. a)  
 1045 OMI NO<sub>2</sub> column (left) and the difference between OMI and CMAQ (right), Unit: Dobson Unit  
 1046 (1 DU = 2.69 × 10<sup>20</sup> molecules/cm<sup>2</sup>); b) OMI HCHO column (left) and the difference between  
 1047 OMI and CMAQ (right), Unit: DU; c) MOPITT near surface CO (left) and the difference  
 1048 between MOPITT and CMAQ (right), Unit:ppbv. Red star in Fig. 7a stands for the proximate  
 1049 location of aircraft campaign.  
 1050 a)



1051  
 1052 b)



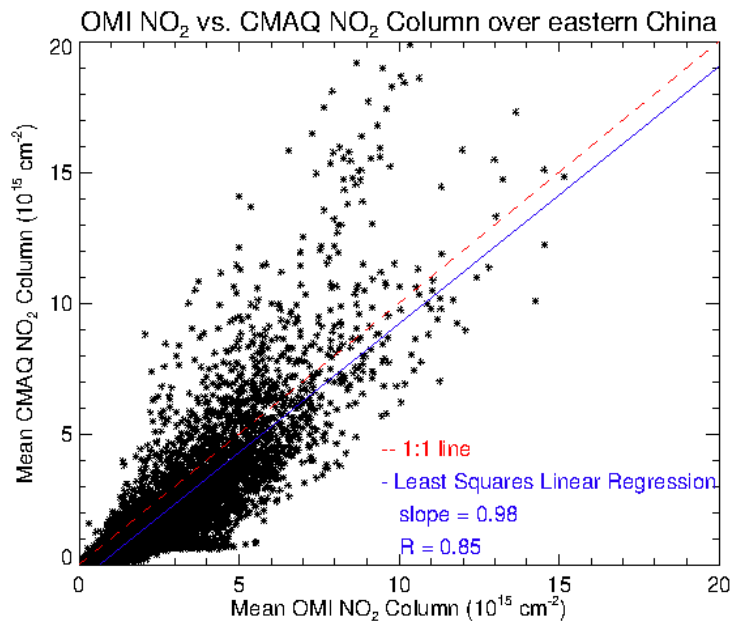
1053  
 1054 c)



1055  
 1056

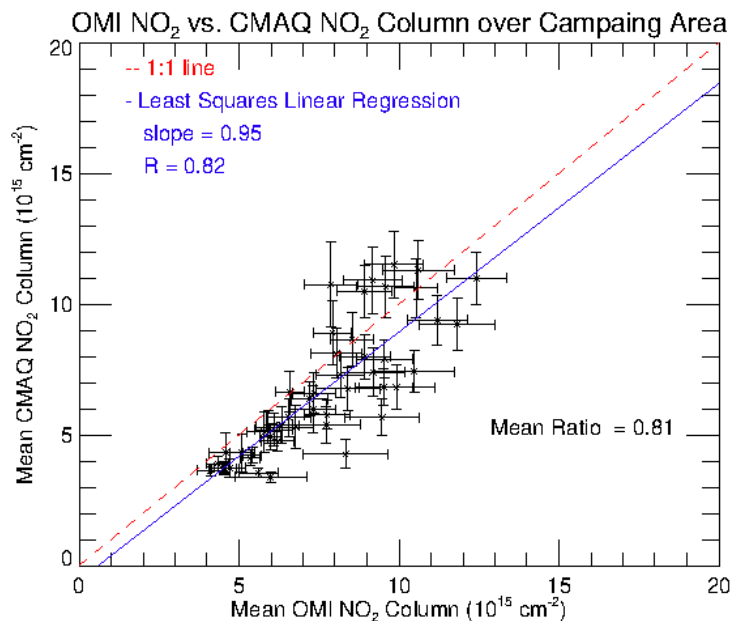
1057 **Figure 8.** Comparison of OMI NO<sub>2</sub> and CMAQ NO<sub>2</sub> columns averaged in May and June 2016.  
1058 a) Scatter plot of NO<sub>2</sub> columns over eastern China; b) Scatter plot of NO<sub>2</sub> columns over the  
1059 campaign area (error bars were calculated as the standard deviation of daily OMI products and  
1060 daily CMAQ simulations during the 2-month campaign).

1061 a)



1062

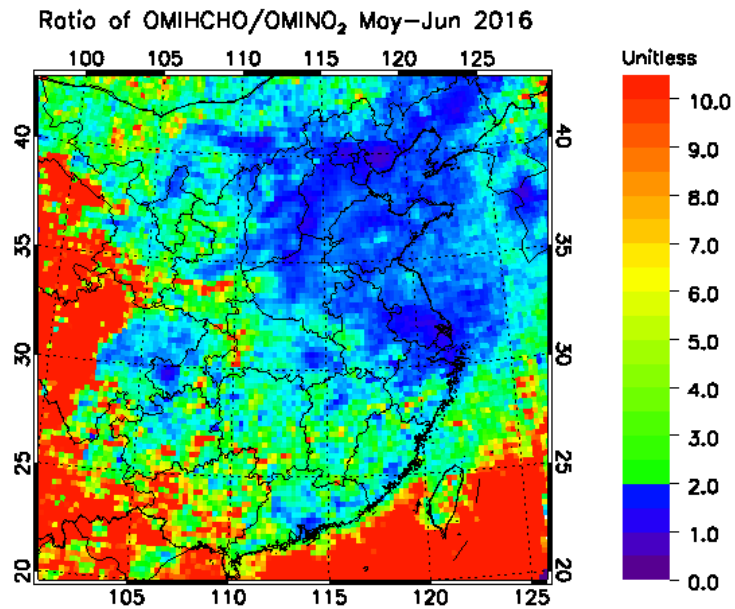
1063 b)



1064

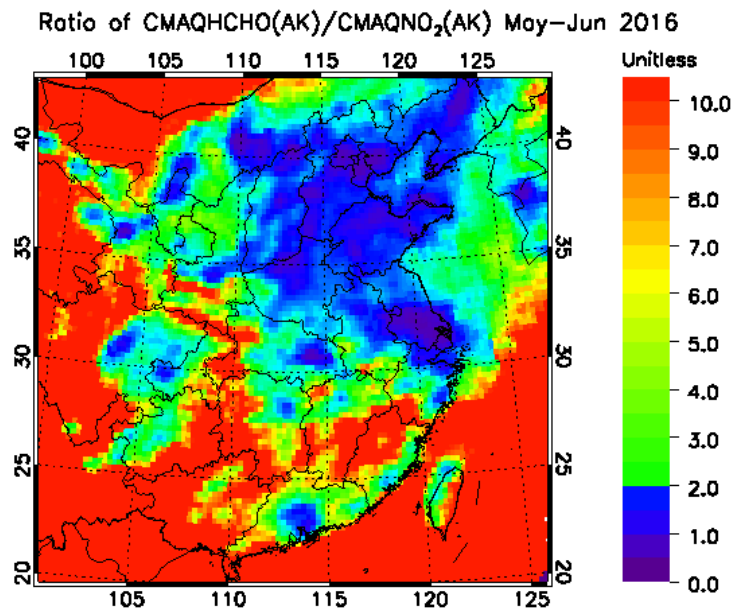
1065 **Figure 9.** Column HCHO/NO<sub>2</sub> ratios over East Asia in spring 2016. a) Ratio derived from  
1066 collocated OMI HCHO and NO<sub>2</sub> observation; b) Ratio calculated from CMAQ HCHO and NO<sub>2</sub>  
1067 simulations with OMI quality information and averaging kernel (AK).

1068 a)



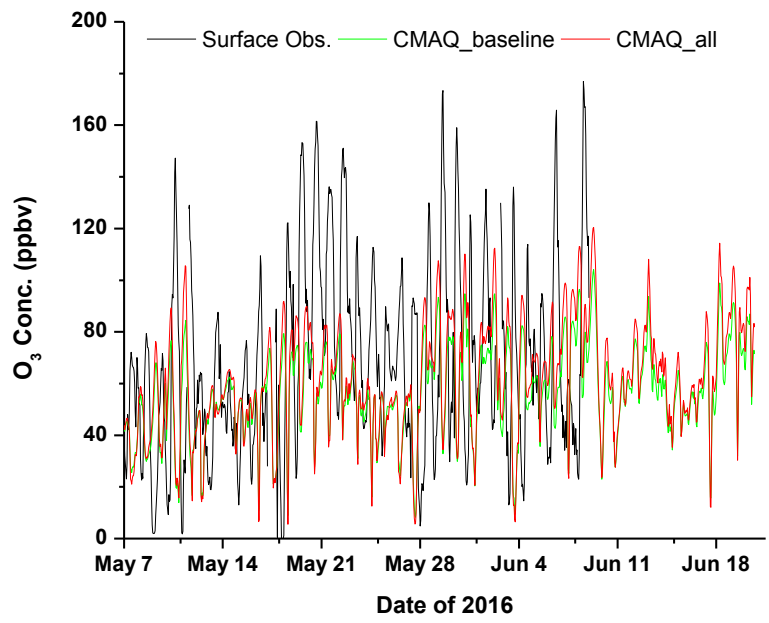
1069

1070 b)

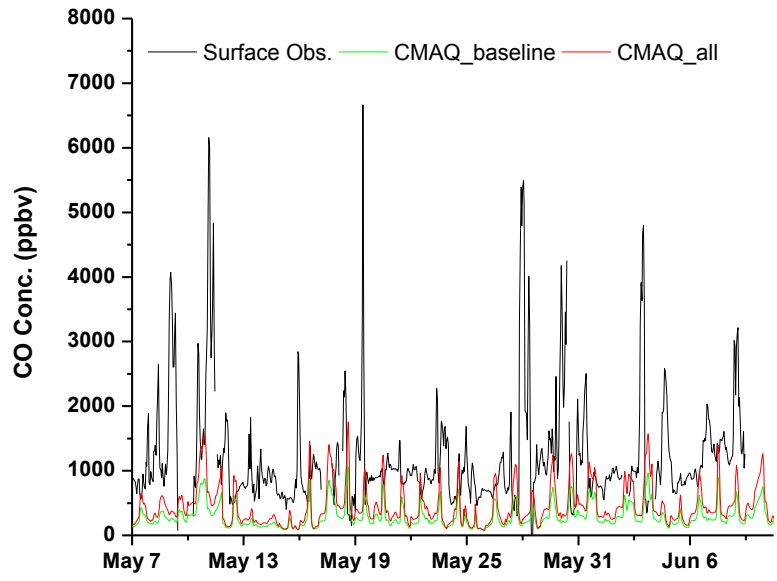


1071

1072 **Figure 10.** Comparison of surface hourly observations of air pollutants and CMAQ simulations  
1073 at the Xingtai supersite from May to mid-June 2016. a) O<sub>3</sub>, b) CO, c) NO<sub>2</sub><sup>\*</sup>, d) NO<sub>x</sub>, and e)  
1074 HCHO. \*Surface NO<sub>2</sub> is inferred as NO<sub>x</sub>-NO from surface observations.  
1075 a)

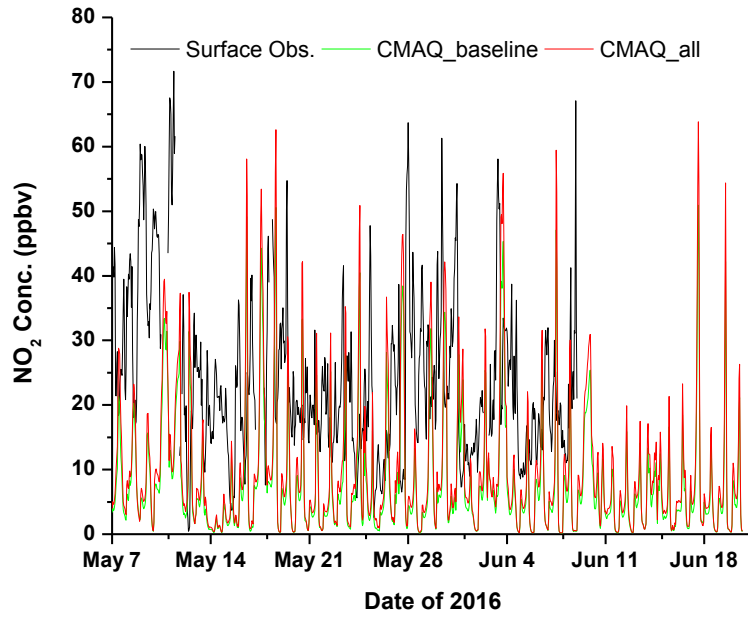


1076 b)  
1077

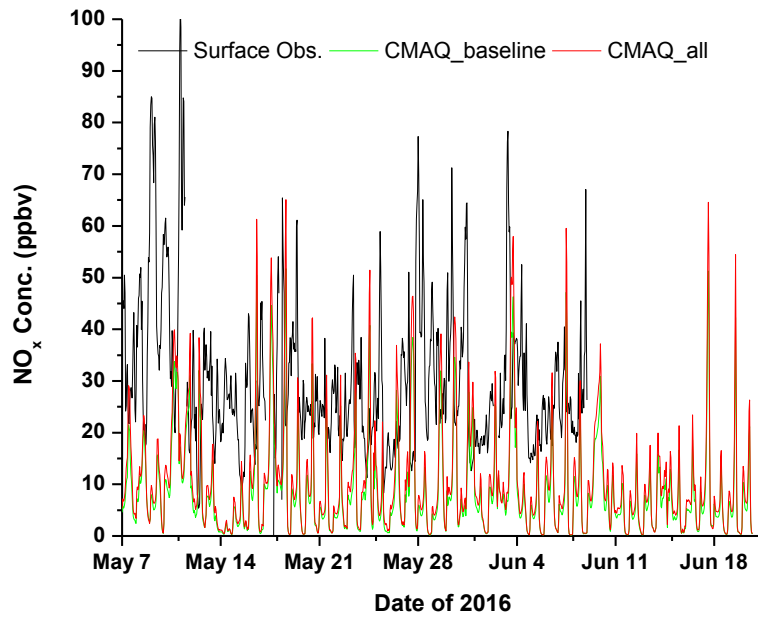


1078

1079 c)

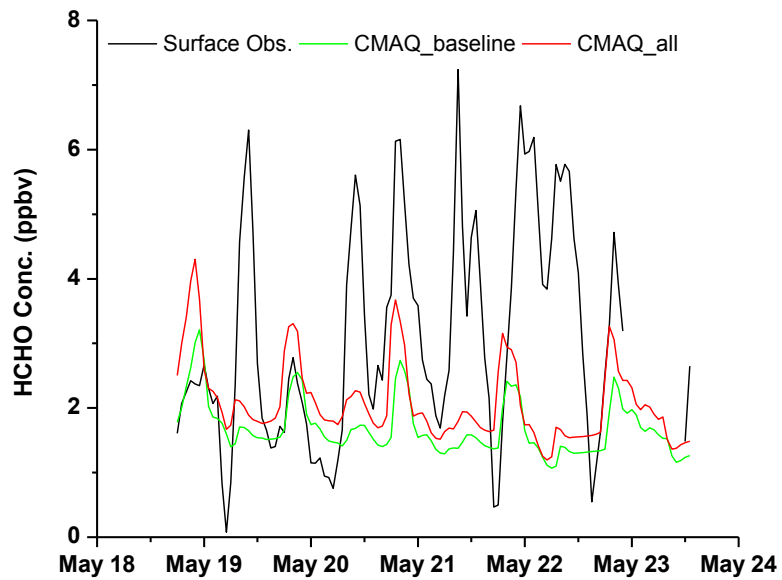


1080  
1081 d)



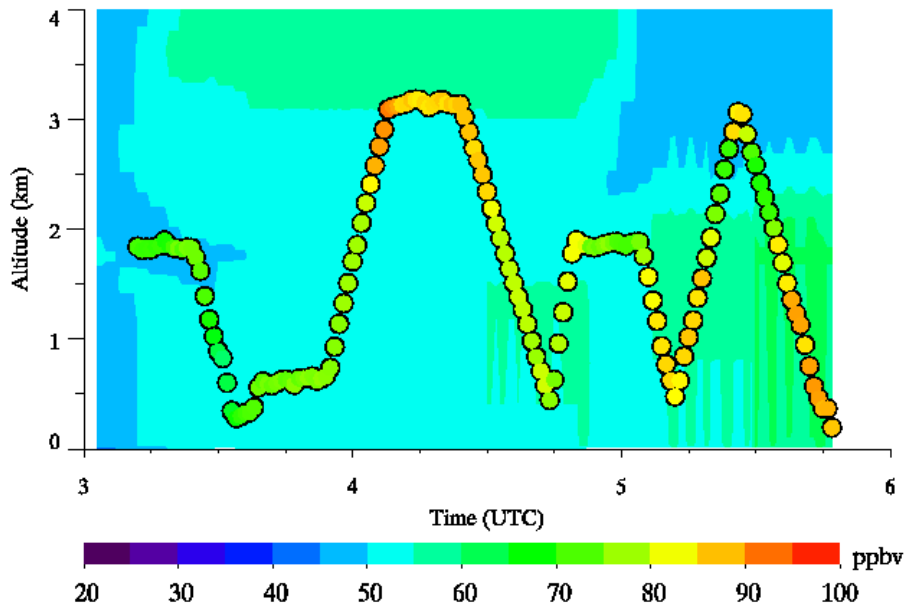
1082  
1083

1084 e)

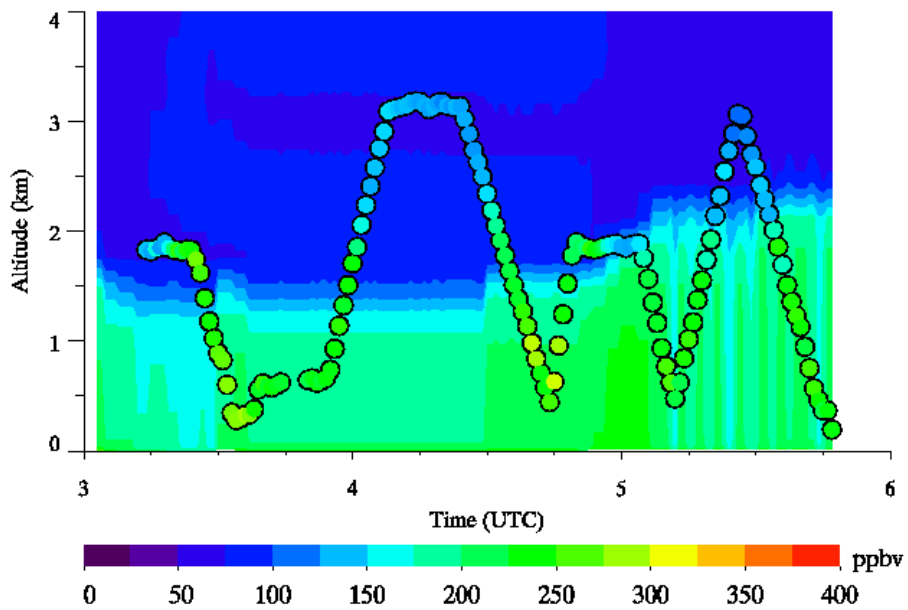


1085

1086 **Figure 11.** A case study comparing aircraft observations and the CMAQ\_All case results on June  
1087 11, 2016. Background: CMAQ simulations. Overlay: 1 min Y12 measurements. a) O<sub>3</sub>, b) CO, c)  
1088 NO<sub>2</sub>, d) NO, and e) NO<sub>y</sub>.  
1089 a)

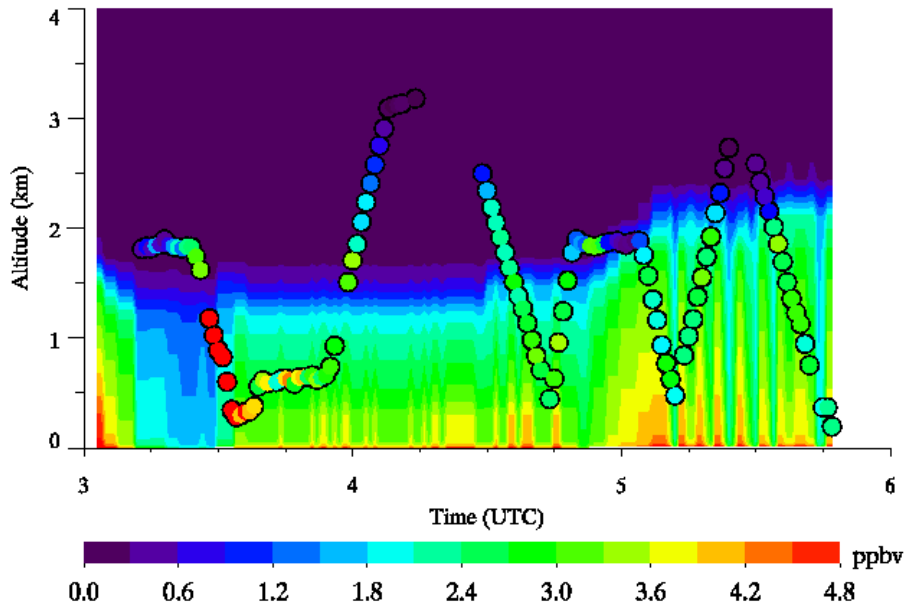


1090 b)  
1091



1092  
1093

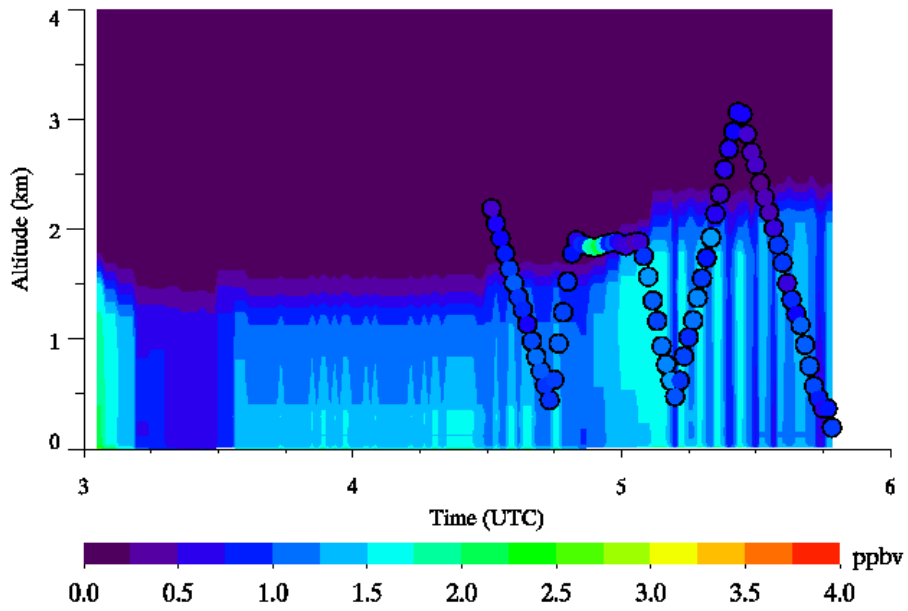
1094 c)



1095

1096

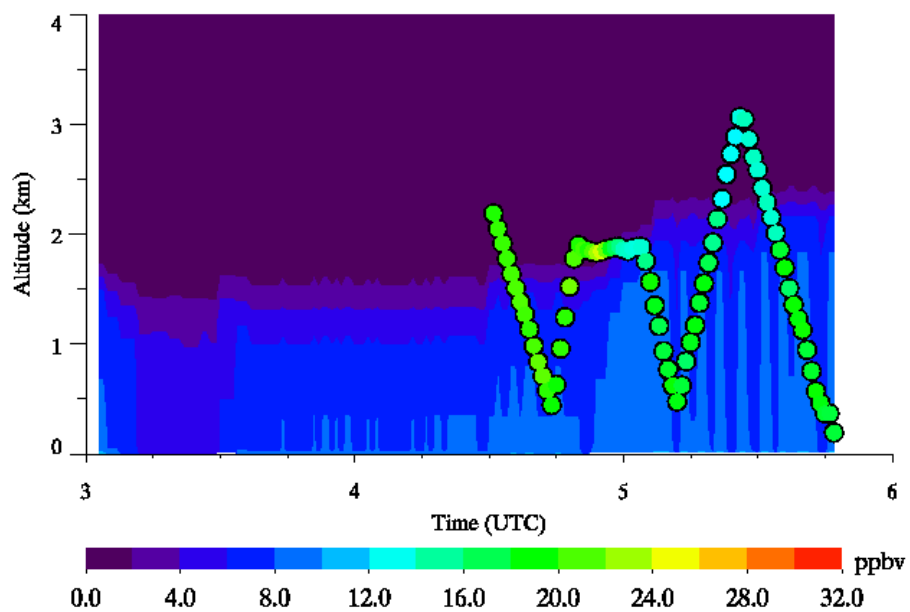
1097 d)



1098

1099

1100 e)



1101